Unconformity-related mineralization and fluid transfers in the northern Aquitaine Basin (France) revealed by fluid inclusions and S-Sr isotopes studies

Loïc Bouat, Pierre Strzerzynski, Véronique Gardien, Guillaume Barré, Yannick Branquet, Jérémie Melleton, Régis Mourgues

Journal of Geochemical Exploration 272 (2025) 107713

Contents lists available at ScienceDirect

Journal of Geochemical Exploration

journal homepage: www.elsevier.com/locate/gexplo

Unconformity-related mineralization and fluid transfers in the northern Aquitaine Basin (France) revealed by fluid inclusions and S-Sr isotopes studies

Loïc Bouat [a,*], Pierre Strzerzynski [a], Véronique Gardien [b], Guillaume Barré [c], Yannick Branquet [d,e], Jérémie Melleton [f], Régis Mourgues [a]

[a] Laboratoire de Planétologie et Géodynamique, UMR6112, CNRS, Le Mans Université, France
[b] Laboratoire de Géologie de Lyon, UMR5276, CNRS, Université Lyon 1, France
[c] Département de géologie et génie géologique, Centre E4M, Université Laval, Canada
[d] Géosciences Rennes, UMR6118, CNRS Université de Rennes, France
[e] Institut des Sciences de la Terre d'Orléans, UMR7237, CNRS, Université d'Orléans, France
[f] Bureau de Recherches Géologiques et Minières (BRGM), Orléans, France

ARTICLE INFO

Keywords:
F-Ba-Pb-Zn(±Ag) deposits
Basement-cover interface
Fluid inclusions
S-Sr isotopic data
Fluid circulation
Extensive Mesozoic geodynamic

ABSTRACT

In sedimentary basins, unconformity between basement and sediments is the ideal site where fluids from different sources can flow and mix, initiating the formation of ore deposits. In western Europe there are numerous F-Pb-Zn-Ba (±Ag, Ge) basin-hosted deposits located near the unconformity between Mesozoic Basins and the Variscan basement as for example the deposits of the Vendée Coast (France) containing fluorite, baryte, pyrite and quartz. Here, microthermometric data on the primary fluid inclusions of these minerals indicate salinity ranging from 1 to 20 wt% eq. NaCl and homogenization temperatures between 100 and 390 °C. We interpret these data as resulting of a fluids circulation in the ore deposit zone, with an early incursion of basin brines expelled by the leaching of Hettangian evaporites buried several tens of kilometers away, followed by an ascent of basement-derived fluids and, finally, a recharge of seawater. In other French deposits, the $\delta^{34}S$ isotopes of baryte are also consistent with a source of fluids from buried evaporites. The $^{87}Sr/^{86}Sr$ ratio of baryte demonstrates a crustal source of elements associated with brines-leached base metals and F—Ba. The process of buried-derived evaporites brines altering the basement along the unconformity is ubiquitous in all unconformity deposits in France.

With our results, we confirm that the basin deposits in the Southeastern Massif Central occur along structures formed during Tethys rifting at around 200 Ma, whereas in the Western part they form at ca. 145 Ma in link with the opening of the Bay of Biscay. This highlights that these basin-hosted deposits are preferentially formed during extensional activity in rifting settings, rather than in compressive settings.

1. Introduction

Hydrothermal deposits in sedimentary basins host most of the world's Pb—Zn reserves (Kyle and Li, 2002), such as the Broken Hill deposit (Wright et al., 1987), the Upper Silesia district (Heijlen et al., 2003), the Kupferschiefer deposits (Blundell et al., 2003; Hitzman et al., 2010), but also REE by-product such as El Hammam (Cheilletz et al., 2010) and Ba deposits in Jebilet (Valenza et al., 2000). Fluid mixing is the main suggested process for hydrothermal mineralization in sedimentary basins (e.g., Anderson, 1975; Corbella et al., 2004; Leach et al., 2005; Muchez et al., 2005; Sverjensky, 1981). This involves the circulation of fluids from water sources as diverse as meteoric, marine and connate waters to fluids related to evaporites, hydrocarbons or magmas (e.g., Boiron et al., 2010; Bons et al., 2014; Lawrence and Cornford, 1995; Sizaret et al., 2009). The movement of these fluids is driven by temperature and/or pressure gradients resulting to subsidence or relief formation (e.g., Garven, 1985; Leach et al., 2010; Oliver et al., 2006; Sverjensky, 1986). The drains through which the fluids flow are the microporosity of the sediments (Boiron et al., 2002; Cathelineau et al., 2012), the macroporosity of rocks such as karsts (Corbella et al., 2006;

* Corresponding author.
E-mail address: loic.bouat@univ-orleans.fr (L. Bouat).

https://doi.org/10.1016/j.gexplo.2025.107713
Received 18 January 2024; Received in revised form 25 September 2024; Accepted 8 February 2025
Available online 10 February 2025

Rhodes et al., 1984; Valenza et al., 2000) and the fracture network including faults (Bons, 2001; Blundell et al., 2003).

Hydrothermal deposits in general and unconformity-related deposits in particular, result from unusual mixing of different fluids enabled by geodynamics (Ingebritsen and Appold, 2012). Due to different driving forces and drainages, fluid flows can be sequenced, as paragenetic and geochemical analysis show (Boiron et al., 2002; Munoz et al., 1994; Walter et al., 2018). To better understand how these deposits were formed, it is therefore necessary to properly define the fluid sources and their sequence of circulation.

In France, unconformity-related deposits have been studied to trace fluid sources, driving forces and drains (Boiron et al., 2002, 2010; Corbella et al., 2004; Heijlen et al., 2003; Hitzman et al., 2010; Leach et al., 2006; Muchez et al., 2005). The work of Valenza et al. (2000), Sizaret et al. (2009), Aquilina et al. (2011) and Laurent et al. (2020) have shown that baryte is a key mineral to track these different parameters during the formation of such deposits. Baryte associated with quartz and calcite is found in the ore deposits on the unconformity of the Vendée Coast (France). The study of quartz fluid inclusions (FIs) and calcite stable isotope analysis show that the ore deposits result from the mixing of seawater, brines and hot fluids (Cathelineau et al., 2012). Fluids movements takes place along the main structures, i.e. horizontally along the unconformity in porous basal sediments and vertically along normal fault planes cutting the basement (Bouat et al., 2023; Cathelineau et al., 2012; Strzerzynski et al., 2020). However, the chronology and timing of these fluid circulations and the geodynamic context associated with the formation of these ore deposits are not yet well constrained.

The aim of this study is to investigate the formation of these unconformity-related ore deposits. Our multidisciplinary approach combines petrographic observations, analysis of FIs in different minerals, and sulfur and strontium isotopic analyses of baryte. The objective is to highlight the nature, origin and succession of fluids at the origin of the deposits on the Vendée Coast. Sulfur and strontium analyses were extended to unconformity deposits from similar deposits in the Southern Armorican Massif and Massif Central. Previous studies have provided us with the regional geodynamic constraints that enable us to determine the exact timing of the circulations of fluids at the origin of the Western Europe deposits.

2. Geological setting

2.1. Geological setting of Vendée (France)

France's first order geology consists of a Variscan basement made of the Armorican, Central, Vosges and Ardennes massifs covered by the Mesozoic sediments of the Paris Basin, Southeast Basin, Grands-Causses Basin and Aquitaine Basin (Fig. 1a). The Variscan massifs dated from Silurian to Carboniferous ages are the witnesses of the collision between the continents Laurussia and Gondwana after the closure of the Rheic and Central oceans (Ballèvre et al., 2009; Faure et al., 2009; Matte, 1986; Ledru et al., 1989). From the southern domain of the Armorican Massif to the Cévennes (Fig. 1a), the massifs are structured into paragneiss and orthogneiss nappes containing ophiolitic relics (i.e. Lower and Upper Gneiss Units) intruded by late-orogenic calc-alkaline and peraluminous granites (Ballèvre et a., 2009; Faure et al., 2009). The Vendée Coast, south of the Armorican Massif (Fig. 1b), is mainly formed of migmatitic orthogneiss, gneissic micaschists and micaschists. Here, the late orogenic WNW-ESE extension characterized by ductile to brittle deformation (Turrillot et al., 2011) and associated with HT-LP metamorphism is well preserved (Cagnard et al., 2004; Goujou et al., 1994; Iglesias and Brun, 1976).

The intracontinental marine basins that opened on the Variscan basement during the Mesozoic (Barbarand et al., 2020; Brunet, 1984; Brunet and Le Pichon, 1982; François et al., 2020), are witness to the opening of the Tethys Rift in the Lower Jurassic for the southeastern basins (Handy et al., 2010; Lemoine et al., 1986; Stampfli and Borel, 2002) and of the Bay of Biscay in the west during the Lower Cretaceous (Jammes et al., 2009). Convergence between Iberian and Eurasian plates in the Upper Cretaceous generated compression that formed retro-foreland basins in the southern Aquitaine Basin (Biteau et al., 2006; Ortiz et al., 2020) and the South-East Basin (Handy et al., 2010; Lemoine et al., 1986; Stampfli and Borel, 2002). Jurassic sediments deposited in the Aquitaine and the South-East Basins are continental detrital to marine carbonate platforms (Barbarand et al., 2020; Biteau et al., 2006; Curnelle and Dubois, 1986). On the Vendée Coast (Fig. 1b), Jurassic transgression is recorded with basal Hettangian detrital sediments (SU1-unit), Hettangian-Sinemurian dolomitic sediments (SU2-unit), Pliensbachian limestones with clay layers (SU3-unit), Toarcian-Aalenian shales (SU4-unit) and thick Bajocian-Callovian limestones (Fig. 1b,

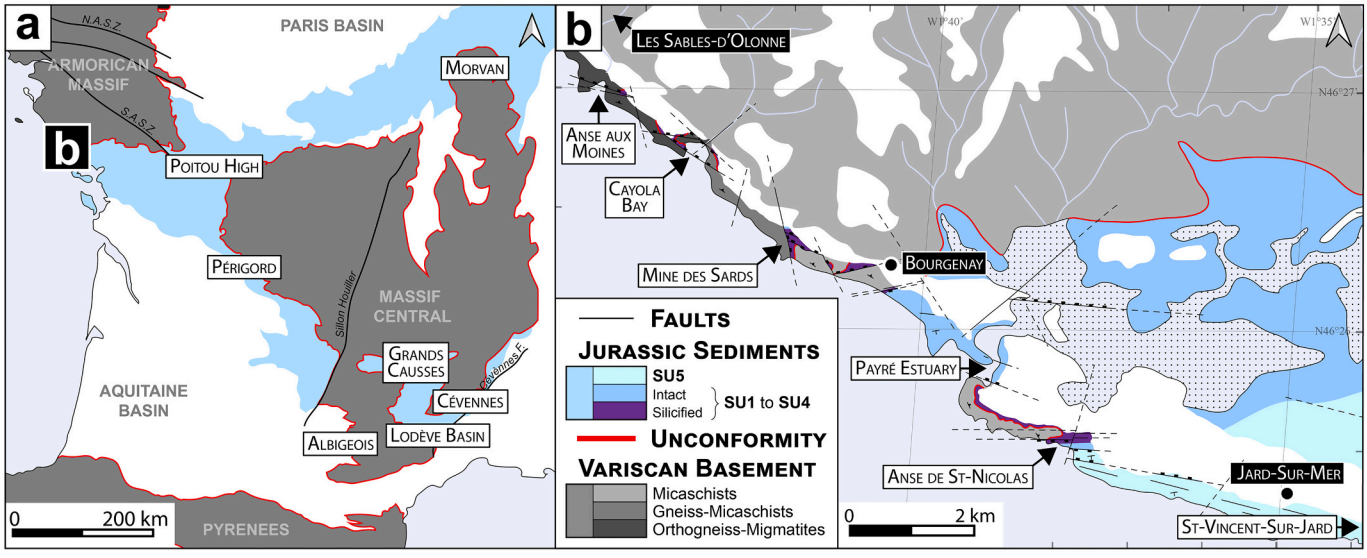

Fig. 1. Location of unconformity-related ore deposits between Variscan massifs and Jurassic sediments (white area representing post-Jurassic sediments). a: Simplified geological map of western France with Ba-F-Pb-Zn deposits districts (the framed "b" corresponds to the location of the detailed Fig. 1b). N.A.S.Z. and S.A.S.Z.: North and South Armorican Shear Zone, respectively, Cévennes F.: Cévennes Fault. b: Detailed geological map of the Vendée Coast (modified from Bouat et al., 2023). Mineralized ore districts/deposits are labeled from 1 to 7 on (a) and from 8 to 13 for the Vendée coast on (b).

SU5-unit; see sedimentary details in Bouat et al., 2023). An interstratum karst level in unit SU2 is reported in relation to a minor emersion dated to the Late Hettangian and Early Sinemurian (Fauré and Bohain, 2017). Upper Jurassic to Upper Cretaceous sediments are absent from the Vendée Coast due to Cretaceous and Cenozoic regressions that lead to emersions (Goujou et al., 1994).

2.2. Unconformity-related ore deposits

France hosts numerous unconformity-related deposits, grouped into districts, all located near the unconformity between Variscan massifs and Mesozoic sediments (Fig. 1). Bordering the Massif Central (Fig. 1a), we find the Morvan district (5.5Mt fluorite reserve; Gigoux et al., 2016) to the north, the Cévennes district (among the major Pb—Zn district in Europe; Muchez et al., 2005) to the south-east, the Grands-Causses (Pb-Zn-Ba deposits) and Albigeois (3.5Mt fluorite past-production; Munoz et al., 2005) districts to the south and the Périgord district (Pb-Zn-Ba deposits) to the west. Between the Armorican Massif and the Massif Central, lies the Poitou High district (Pb-Zn ± Ag deposits; Boiron et al., 2010; Cathelineau et al., 2012) and, south of the Armorican Massif, the Vendée Coast district (Ba-Pb-Zn ± Ag; Goujou et al., 1994).

These mineral deposits located on unconformity are made up of similar baryte, quartz, fluorite, galena and sphalerite parageneses dating from the Triassic to Lower Cretaceous (Bonhomme et al., 1987; Cathelineau et al., 2012; Gigoux et al., 2015; Munoz et al., 2005; Bouat et al., 2023). These deposits correspond either to veins hosted in the basement beneath the unconformity and/or in the sedimentary cover, or to stratiform and karst-fill mineralization. The fluids responsible for their formation are of shallow origin, with temperatures between 60 and 160 °C and salinities between 0 and 25 wt% eq. NaCl (Cathelineau et al., 2012; Gigoux et al., 2016; Laurent et al., 2020; Léost et al., 1999; Munoz et al., 1999; Sabouraud et al., 1980; Sizaret et al., 2004).

In the Vendée Coast districts, ore deposits consist of baryte, quartz, pyrite and a minor amount of Ag-rich galena and sphalerite attesting of hot fluid up to 280 °C (Cathelineau et al., 2012). Previous mining works have identified zones containing 0.36 % Pb, 0.19 % Zn and 45 g/t Ag (Goujou et al., 1994). Mineralization occurs in karsts and NW-SE basement fractures and in the units SU1 to SU3-unit (Bouat et al., 2023). Calcite-filled NW-SE fractures are dated by U—Pb at 145 Ma by Bouat et al. (2023). Associated with these deposits, the basement is affected by alteration below the unconformity (Cathelineau et al., 2012; Strzerzynski et al., 2020) and above, the cover is strongly silicified (Fig. 1b; Bouat et al., 2023; Cathelineau et al., 2012).

3. Methods

3.1. Sampling strategy

In this study, we analyzed 22 samples from the Vendée Coast. They are representative of all zones and are characterized either by disseminated minerals hosted in the SU2-unit, or by NW-SE trending veins crosscutting all formations (the basement and SU2 to SU5-units) or, filling karsts in the SU2-unit (Fig. 1b; Table 1). Among these samples, 10 samples were studied for fluid inclusions microthermometry, 8 samples for strontium isotopes and 13 for sulfur isotopes.

For comparison, 8 samples of baryte from veins crosscutting the basement near the unconformity and the sedimentary cover (Fig. 1a; Table 1) from ore deposits in the Périgord (Guillot et al., 1979), the Grands-Causses (Briand et al., 1979, 1993; Legendre et al., 2009; Mennessier and Collomb, 1986; Roig et al., 2002) and the Cévennes districts (Alabouvette et al., 1988). These samples were part of the 1970s France mining inventory collection of the B.R.G.M. (French geological survey). In this study, these samples were studied for strontium and sulfur isotopes.

3.2. Fluid inclusions microthermometry

The paragenetic sequence of the deposits on the Vendée Coast was first obtained by observing the minerals in the field, then using a LEICA DM750P optical microscope. Microthermometric analyses were performed on a Linkam MDS600 heating/freezing stage connected to an Olympus BH2 binocular microscope at the LGL-TPE laboratory (Lyon). Calibration was based on phase transition temperatures measurments on FIs of synthetic samples of pure H_2O (melting temperature of ice, $T_{m\ pure\ H2O} = 0$ °C, homogenization temperature, $T_{h\ pure\ H2O} = +374$ °C) and H_2O-CO_2 (melting temperature of pure CO_2, $T_{m\ CO2} = -56.6$ °C, melting temperature of CO_2-clathrate, $T_{m\ CO2\text{-}Clath} = +10$ °C). Salinity is calculated in weighted percent equivalent of NaCl (wt% eq. NaCl) from the ice melting temperature of the FIs using the Bodnar (1993) relationship for NaCl-H_2O systems. To avoid cracking through the twining and decrepitation of FIs, the microthermometric measurements on fluorite and baryte followed a single heating-cooling cycle.

3.3. Isotopic ratio $^{87}Sr/^{86}Sr$ analysis on baryte

Samples were collected using a Dremel® tool to drill holes to precisely separates the crystals from the host-rock and to make 50-500 mg of an extremely fine powder (<250 μm). The $^{87}Sr/^{86}Sr$ isotopic ratio of baryte was performed at Laboratory Géosciences Rennes using a Finnigan MAT-262 seven-collector mass spectrometer. Each sample was partially dissolved in a mixture of hydrofluoric and nitric acids, then dried and taken up with concentrated hydrochloric acid. Sr separation was performed by cation exchange columns chromatography using BioRad AG50W-X8 resin. Calibration was carried out using Sr standard NBS-987 ($^{87}Sr/^{86}Sr = 0.710250$). Mass fractionation was checked using the value of 8.3752 for $^{88}Sr/^{86}Sr$. Blanks analyses gave values <100 pg for Sr and are therefore considered negligible.

3.4. Sulfur isotopic content on baryte and sulfide

The sulfur isotopic composition ($\delta^{34}S$) of baryte and pyrite from the Vendée Coast and baryte from other unconformity-related ore deposits was measured online using a Thermo Scientific EA IsoLink IRMS System at CRPG laboratory (Vandoeuvre les Nancy, France). A quantity of 0.7 mg of each sample was enclosed in tin capsules to which approximatively 0.5 mg of vanadium pentoxide was added. The tin capsules were then transferred to an autosampler and burned at 1020 °C in a combustion reactor consisting of a quartz tube filled with tungsten oxide and pure copper. The gases produced (N_2, CO_2 and SO_2) were separated on a chromatographic column, and the isotopic composition of the sulfur was measured using a Thermo Scientific Delta V Advantage continuous-flow isotope ratio mass spectrometer. The Sulfur isotopic composition ($\delta^{34}S$) of the sulfates was obtained by comparison with three international standards regularly included in the analysis: (i) IAEA SO6 ($\delta^{34}S = -34.1$ ‰), (ii) IAEA SO5 ($\delta^{34}S = +0.5$ ‰) and (iii) NBS 127 ($\delta^{34}S = +20.3$ ‰). The sulfur isotopic composition ($\delta^{34}S$) of the sulfides was determined by comparison with three international standards regularly included in the analysis: (i) IAEA S1 ($\delta^{34}S = -0.3$ ‰), (ii) IAEA S2 ($\delta^{34}S = +22.62$ ‰) and (iii) IAEA S3 ($\delta^{34}S = -32.49$ ‰). Values are quoted in the delta notation in ‰ versus VCDT and reproducibility was better than 0.3 ‰.

4. Results

4.1. Vendée Coast deposits paragenetic sequence

Based on field and microscopic observations, 6 stages of mineralization have been distinguished in 6 outcrops on the Vendée Coast (Fig. 1b and Fig. 2). Only the Anse de St-Nicolas site presents the entire paragenetic sequence (i.e. the 6 stages). Stage 1 and 2 correspond to pervasive mineralization disseminated in the sediments while stage 3 to

Table 1
Studied samples with localities, mineral association, morphologies, FIs data on samples form the Vendée Coast and isotope data on all samples. Qz: quartz, Py: pyrite, Brt: baryte, Fl: fluorite, Mrc: marcasite, Gn: galena, Sp: sphalerite, Cal: calcite, Ccp: chalcopyrite. Labeled minerals refer to the paragenetic stage (Fig. 2).

District	Zone	Host-rock	Mineral	Morphology	Sample	Number	Salinity (wt% NaCl)		T_h (°C)		$^{87}Sr/^{86}Sr$	$\delta^{34}S$ (vCDT ‰)
							Mean	Range	Mean	Range		
Vendée Coast	Anse aux Moines	Orthogneiss (near unconformity)	Qtz5	NW-SE vein	AM2	10	6.7 ± 1.4	4.9 to 12.5	249.2 ± 39.4	169.6 to 332.8		
	Cayola Bay	Silicified SU2	Qtz5	Karst	QCAY	3	6.4 ± 1.0	4.9 to 7.7	231.2 ± 45.2	163.4 to 274.4		
	Mine des Sards	Silicified SU2	Qtz5	NW-SE vein	MS11	14	9.2 ± 3.8	3.6 to 18.4	257.7 ± 70.7	160.2 to 394.1		
			Py5	NW-SE vein	MS301							−23.0 ± 0.5
	Payré Estuary	SU2	Brt4	NW-SE vein	PPX						0.709692 ± 1.0E-5	
					PN201						0.709787 ± 0.9E-5	+26.7 ± 0.6
	Anse de	Micaschists (near unconformity)	Brt4	NW-SE vein	min4						0.710900 ± 1.0E-5	+24.9 ± 0.6
	St-Nicolas	Silicified SU2	Fl2	Disseminated	Pt167a	4	17.5 ± 3.6	13.3 to 21.2	132.8 ± 21.9	110.4 to 173.1		
			Brt4	Karst	GA4	8	7.2 ± 1.7	3.8 to 10.6	304.9 ± 39.6	243.0 to 378.0		
					K1	2	6.9 ± 0.7	6.2 and 7.6	227.3 ± 32.1	195.2 and 259.4		
					21						0.710751 ± 1.0E-5	+27.6 ± 0.6
				NW-SE vein	25						0.710363 ± 1.0E-5	+25.0 ± 0.6
					PP9						0.710126 ± 1.0E-5	+23.5 ± 0.6
					Pt201						0.710093 ± 1.0E-5	+28.6 ± 0.6
			Py5	NW-SE vein								−23.5 ± 0.5
					Pyrite-St-Nicolas							−12.7 ± 0.5
			Qtz5	Karst	GA3	13	6.8 ± 2.6	2.7 to 12.9	272.8 ± 61.6	166.0 to 384.8		
					QSN	5	4.6 ± 0.2	4.3 to 4.9	191.7 ± 24.5	145.8 to 230.2		
				NW-SE vein	20	5	3.6 ± 2.6	1.0 to 7.1	273.1 ± 56.3	140.9 to 366.2		
					Pt201b	4	6.9 ± 1.0	5.3 to 8.7	235.0 ± 15.4	204.3 to 260.1		
		SU5	Brt4	NW-SE vein	II							+27.2 ± 0.6
			Mr	Nodule	MR202							−36.9 ± 0.5
	Jard-Sur-Mer	SU5	Brt4	NW-SE vein	MR201						0.709581 ± 1.0E-5	+43.6 ± 0.6
			Py5	NW-SE vein								−7.3 ± 0.5
Périgord	Neuil	Gneiss with plagioclase and mica (near unconformity)	Qtz-Gn ± Brt	NW-SE veins	JM11						0.708969 ± 1.0E-5	+20.7 ± 0.6
Grands-Causses	Kaymard	Sericitic schists (near unconformity)	Qtz-Fl-Brt ± Gn	WNW-ESE veins	JM4						0.710136 ± 1.3E-5	+20.0 ± 0.6
	St-Geniez d'Olt	Micaschists (near unconformity)	Brt	NW-SE veins	JM2						0.710685 ± 1.1E-5	+23.8 ± 0.6
	Barjac	Lower Jurassic dololimestones	Brt	NW-Se veins	JM8						0.712843 ± 0.9E-5	+23.3 ± 0.6

(*continued on next page*)

Table 1 (*continued*)

District	Zone	Host-rock	Mineral	Morphology	Sample	Number	Salinity (wt% NaCl)		T_h (°C)		$^{87}Sr/^{86}Sr$	$\delta^{34}S$ (vCDT ‰)
							Mean	Range	Mean	Range		
	Allenc	Granite and Lower Jurassic dololimestones	Qtz-Brt-Gn-Sl	NW-SE veins	JM6						0.711998 ± 1.0E-5	+14.2 ± 0.6
	Bleymard	Middle Jurassic limestones	Qtz-Cal-Brt-Gn-Sl	Stratiform, NNW-SSE veins	JM7						0.710639 ± 1.0E-5	+16.9 ± 0.6
	Millau	Lower Jurassic dololimestones	Brt-Gn-Cp	NW-SE veins	ML1b						0.710042 ± 0.9E-5	+14.0 ± 0.6
Cévennes	Malines	Cambrian dololimestones, Triassic shales and Middle Jurassic limestones	Sl-Gn-Brt ± Qtz	Karsts, ENE-WSW veins	JM9						0.710457 ± 1.0E-5	+13.9 ± 0.6

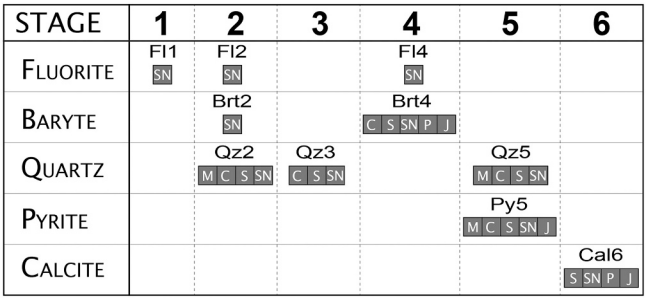

Fig. 2. Paragenetic sequence. Letters refer to mineralized zones from the Vendée Coast (Fig. 1b): M = Anse aux Moines, C=Cayola Bay, S = Mine des Sards, P=Payré Estuary, SN = Anse de St-Nicolas and J = Jard-sur-Mer.

6 are fracture fillings (veins) and karsts (geodes).

The 6 paragenetic stages are defined as follow:

Stage 1 corresponds to disseminated (sometimes clustered) fluorite (Fl1) in silicified SU2 (Fig. 3a). The fluorite crystals take the form of beige, euhedral cubic crystals 100 µm to 0.5 mm wide. Microscopically, the epigenized primary oolites are preserved within the Fl1-crystals (Fig. 3a) but the primary mineral (probably carbonates) is completely pseudomorphosed into fluorite.

Stage 2 corresponds to a second generation of fluorite (Fl2-fluorite), associated with baryte (Brt2) and quartz (Qz2), the cryptocrystalline quartz is responsible for silicification (Fig. 3a-e-i). Stage 2 minerals replace previous oolitic structures and constitute up to 90 % of the rock (Fig. 3a). Fl2-fluorite is yellow and appears either as a growth rim around Fl1-fluorite or, as isolated and/or clustered cubic crystals 100–150 µm wide (Fig. 3a). Brt2-baryte crystals are white and needle-shape from 300 µm to more than a few centimeters, showing the epigenization of bivalve fossils.

Stage 3 is characterized by quartz (Qz3) which consists of a thin overgrowth surrounding Qz2-quartz (Fig. 3a-i).

Stage 4 corresponds to the filling stage of karsts and veins oriented WNW-ESE. The filling consists of rare 0.5 mm wide yellow euhedral cubic crystals of fluorite (Fl4) and baryte (Brt4-baryte). Brt4-baryte consists of white crystals aggregated in crest-like forms (or rosettes) 0.5 cm to 3 cm wide. In karst, it has a cockade morphology (Fig. 3d). In the Mine des Sards, isolated boxworks of crested aggregates in karsts have already been reported (Bouat et al., 2023). In the veins Brt4-baryte shows a syntaxial growth (Fig. 3b-c).

Stage 5 corresponds to a second episode of veins and karsts filling. It is composed of euhedral crystals of pyrite (Py5-pyrite) and quartz (Qz5-quartz). In WNW-ESE oriented veins, Py5-pyrite forms thin layers (≤1 cm) overlying Brt4-baryte (Fig. 3b-d) or between Qz3-quartz and Qz5-quartz (Fig. 3e). In Anse de St-Nicolas, Py5-pyrite fills NNW-SSE fractures cutting WNW-ESE oriented Brt4-baryte veins (Fig. 3c). In SU5 unit, WNW-ESE oriented lenticular Brt4-baryte and Py5-pyrite mineralization outcrops on the beach west of Jard-sur-Mer harbor. The Qz5-quartz consists of large euhedral crystals 100 µm to a few centimeters long (Fig. 3e-i) covering the Brt4-baryte in the karsts (Fig. 3d). It appears in single-mineral veins or in association with Brt4-baryte and Py5-pyrite (Fig. 3e).

Stage 6 corresponds to euhedral calcites (Cal6) filling the veins (Fig. 3f). Calcite Cal6- is not observed in the basement, is rare in the silicified SU2-unit and ubiquitous in the fractures of non-silicified SU2, SU3 and SU5 units. U—Pb dating of Cal6-calcite gives two distinct ages of growth at 145 and 70–80 Ma respectively (Bouat et al., 2023).

4.2. *Vendée Coast deposits fluid inclusions analysis*

FIs analyzes were conducted on Fl2-fluorite, Brt4-baryte and Qz5-quartz. Microscopic observations on these minerals hosted in the basement and mainly in the silicified SU2, show that their primary FIs are biphasic, with a liquid and vapor phases (Fig. 3 g-h-j). Vapor volume is between 10 and 15 % in FIs of Fl2-fluorite, between 15 and 20 % in FIs of Brt4-baryte and around 20 % in FIs of Qz5-Quartz. No secondary FIs in trails or different FIs populations in the same sample were observed. Microthermometric analysis of the FIs of Fl2-fluorite, and Brt4-baryte samples analyzed are from the Anse de St-Nicolas deposit (Fig. 1b). Qz5-Quartz samples are from the Anse aux Moines, Cayola Bay, Mine des Sards and Anse de St-Nicolas deposits (Fig. 1b). All microthermometric data are available in supplementary materials (Table S1) with histograms (Fig. S1).

Translucent Fl2-fluorite crystals host irregularly shaped FIs 15 to 30 µm wide (Fig. 3 g). Brt4-baryte crystals form white crest-like span hosting numerous solid inclusions and FIs making them difficult to observe (Fig. 3 h). The FIs have an elongated shape (up to 40 µm long) and are preferably oriented along the crystal's c-axis. In Qz5-quartz crystals, FIs are rare, up to 25 µm wide and randomly scattered.

Microthermometric data are reported in Table 1 and Fig. 4. Ice melting temperatures (T_m) range from −18.2 °C and − 0.4 °C indicating salinities ranging between 21.2 and 1.0 wt% eq. NaCl, respectively. Homogenization temperatures (T_h) in the liquid phase range from 110.4 °C to 394.1 °C depending on the host-mineral.

In Anse de St-Nicolas, FIs of Fl2-fluorite have the highest salinity (13.3 to 21.2 wt% eq. NaCl) and the lowest T_h ranging between 110.4 °C and 173.1 °C (Table 1; Fig. 4a). Brt4-baryte FIs are the least saline (4.0 and 9.5 wt% eq. NaCl) but have the highest T_h ranging from 195.2 °C to 378.0 °C (Table 1; Fig. 4a). In Qz5-quartz, FIs have highly variable salinities (between 1.0 and 12.9 wt% eq. NaCl) and T_h value ranging between 140.9 and 384.8 °C (Table 1; Fig. 4a). Microthermometry data for FIs contained in a single Qz5-quartz crystal and positioned along the crystal'sc-axis show a decrease of both salinities from 10.0 to 3.2 wt% eq. NaCl and T_h from 378.9 to 215.7 °C, respectively (Fig. 3i-j). In Mine des Sards, FIs in Qz5-quartz, have the most dispersed salinity and T_h,

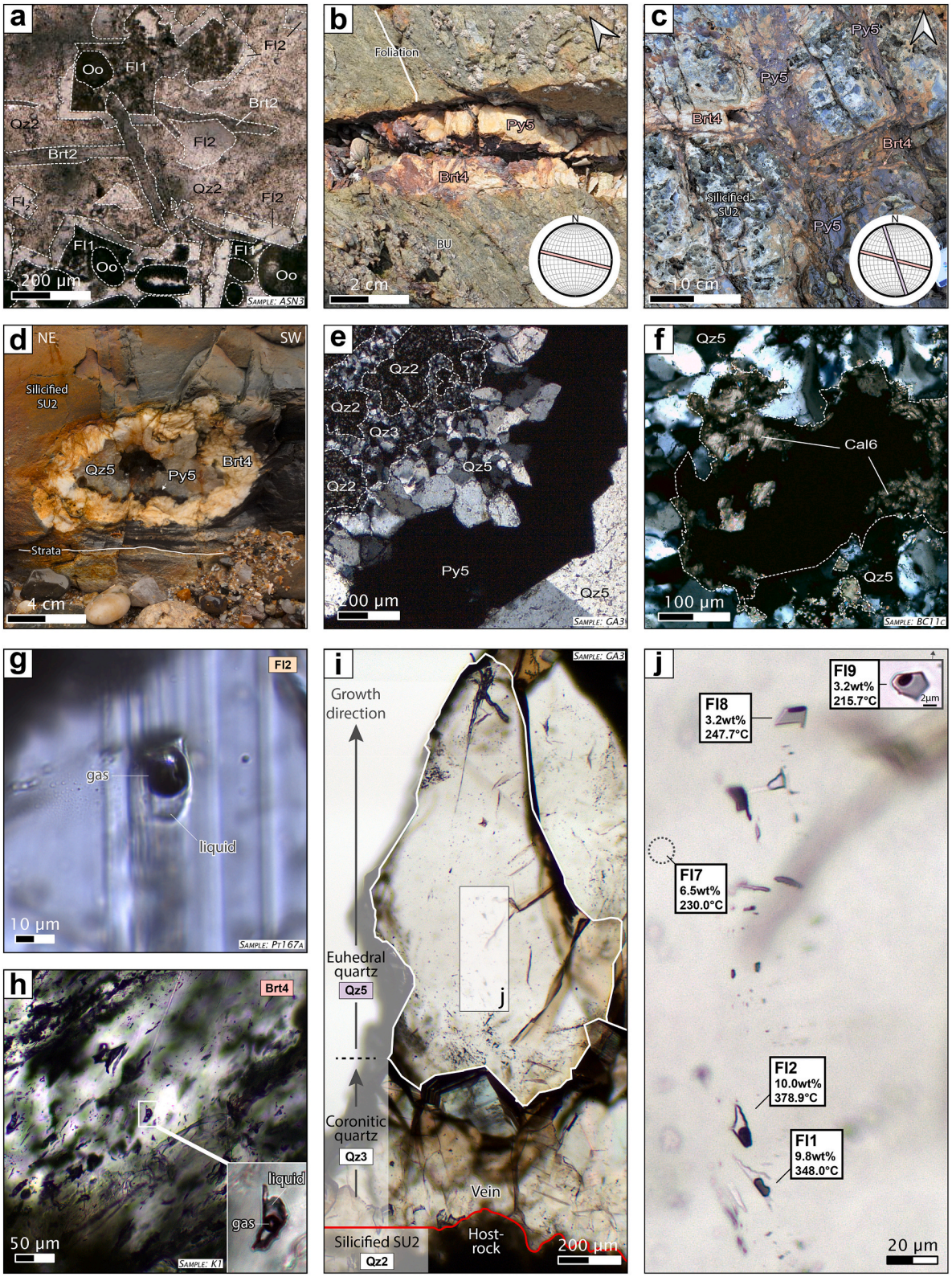

Fig. 3. a: Disseminated Fl1-fluorite in association with epigenized oolites (Oo) with Fl2 overgrowth, Fl2-fluorite crystals, Brt2 in needle-shape and cryptocrystalline Qz2 hosted in SU2. b: Basement-hosted WNW-ESE Brt4-baryte vein. c: WNW-ESE Brt4-baryte vein hosted in SU2- and crosscut by NNW-SSE Py5-pyrite vein. d: karst filled by Brt4-baryte, Py5-pyrite and Qz5-quartz hosted in SU2. e: Vein with silicified clasts (Qz2) with a rim of Qz3 on the wall and larger Qz5-quartz crystals with Py5-pyrite in the core. f: Vug in a Qz5-quartz vein filled by Cal6. g: Representative FI in Fl2-fluorite. h: Representative FIs in Brt4-baryte. i-j: Representative FIs in Qz5-quartz. In (j), FIs salinity and Th values are reported, showing a decreasing of salinity and Th along the crystal growth direction.

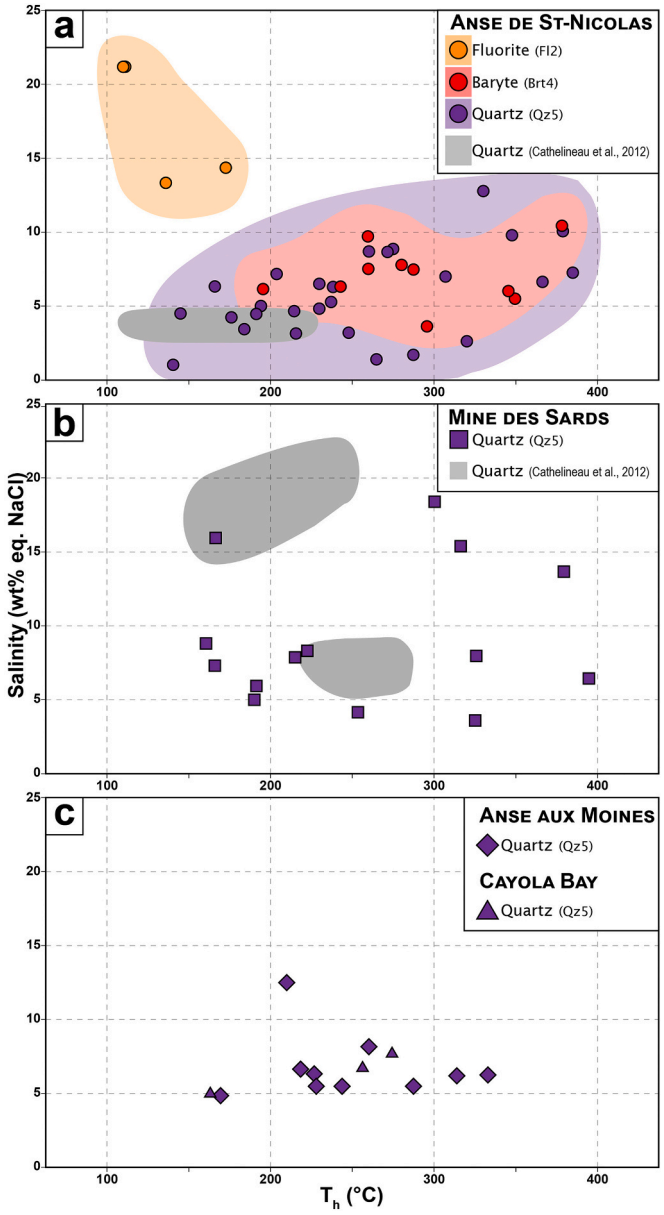

Fig. 4. Salinity vs T_h diagram for FIs from (a) Anse de St-Nicolas, (b) Mine des Sards and (c) Anse aux Moines and Cayola Bay (Table 1).

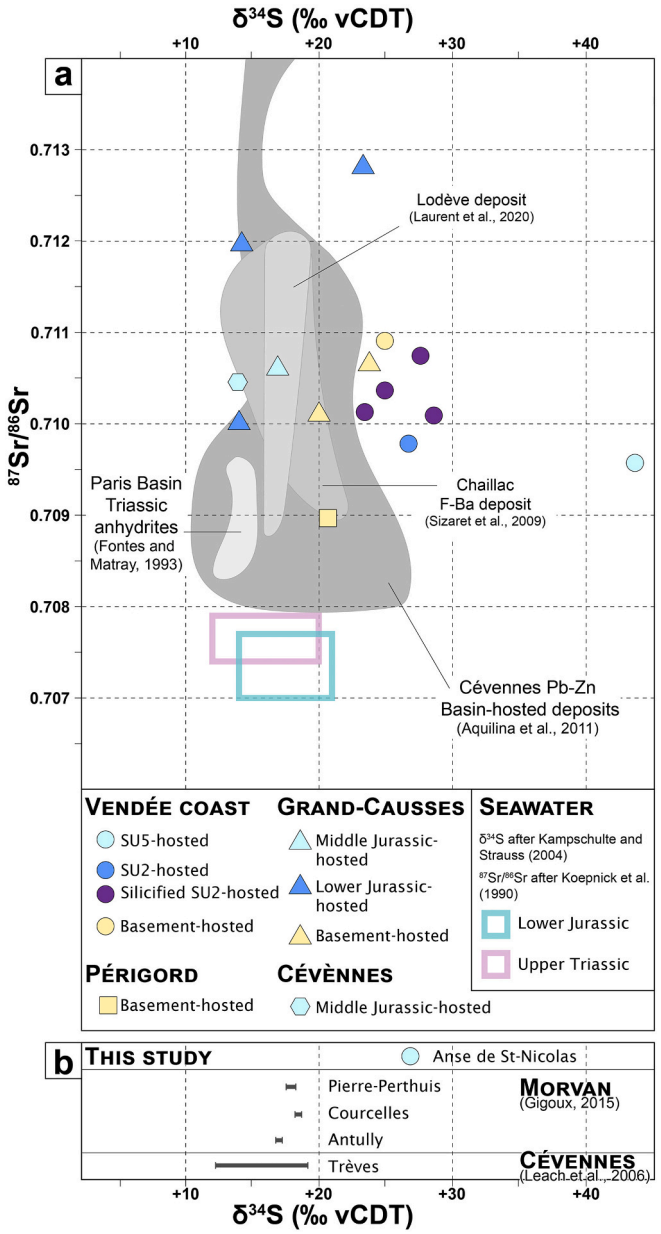

Fig. 5. a: $^{87}Sr/^{86}Sr$ vs $\delta^{34}S$ plot for Brt4-baryte samples from the Vendée coast and baryte samples from other districts (see Table 1). Shaded area and boxes represent literature data. b: $\delta^{34}S$ plot for baryte samples. Brt4-baryte samples correspond to the SU5 sample from Anse de St-Nicolas (see Table 1).

ranging from 3.6 to 18.4 wt% eq. NaCl and from 160.2 to 394.1 °C, respectively (Table 1; Fig. 4b). For the same generation of Qz5-quartz, at Anse aux Moines and Cayola Bay (Table 1; Fig. 4c), the FIs have a salinity between 4 and 12.5 wt% eq. NaCl and T_h between 160 and 335 °C.

4.3. $^{87}Sr/^{86}Sr_{baryte}$ and $\delta^{34}S_{baryte\text{-}sulfide}$

$^{87}Sr/^{86}Sr$ and $\delta^{34}S$ analyses of Brt4-baryte and Py5-pyrite samples from the Vendée Coast district were carried out (Table1; Fig. 5a) and compared with analyses of baryte samples from unconformity-related around the Massif Central (Table 1; Fig. 1a). The $^{87}Sr/^{86}Sr$ ratio and $\delta^{34}S$ values of Brt4-baryte vary from 0.709581 to 0.710900 and from +23.5 to +43.6 ‰ respectively (Table 1; Fig. 5a). The $^{87}Sr/^{86}Sr$ ratio vary according to the host-rock (Fig. 5a). Basement Brt4-baryte has the highest value (0.710900), while the lowest value of 0.709581 corresponds to the Brt4-baryte hosted in SU5- at the top of the stratigraphic sequence (Fig. 5a). The $^{87}Sr/^{86}Sr$ ratio of Brt4-baryte from SU2 shows mean values between 0.709692 and 0.709787 in unaltered SU2 and between 0.710093 and 0.710751 in silicified SU2 (Table 1; Fig. 5a). Brt4-baryte $\delta^{34}S$ values of are clustered around +25 ‰ in basement embedded and SU2 samples and increase to +27.2 and + 43.6 ‰ in SU5 (Table 1; Fig. 5a-b). A sedimentary marcasite nodule in SU5 shows highly depleted $\delta^{34}S$ value at −36.9 ‰, while Py5-pyrite in SU2 and SU5 units is less depleted with values at −23.5 ‰ and − 7.3 ‰, respectively (Table 1). $\delta^{34}S$ values were obtained on two Brt4-baryte /Py5-pyrite pairs from the silicified SU2 of Anse de St-Nicolas (baryte = +28.6 ‰; pyrite = −23.5 ‰) and SU5 from Jard-Sur-Mer (baryte = +43.6 ‰; pyrite = −7.3 ‰; Table 1), leading to similar $\Delta^{34}S_{pyrite\text{-}baryte}$ at +52.1 ‰ and + 50.9 ‰, respectively.

Baryte samples from other Massif Central districts have $^{87}Sr/^{86}Sr$ and $\delta^{34}S$ values between 0.708969 and 0.712843 and between +13.9 and + 23.8 ‰, respectively (Table 1; Fig. 5a). $^{87}Sr/^{86}Sr$ values differ from district to district and host rocks to host rock. The Périgord baryte

sample hosted in a gneiss (Fig. 1a) has the lowest $^{87}Sr/^{86}Sr$ ratio with a value at 0.708969. In the Grands-Causses (Fig. 1a), baryte samples have $^{87}Sr/^{86}Sr$ ratio ranging from 0.710136 to 0.710685 in the basement. In the overlaying Lower and Middle Jurassic sedimentary series, $^{87}Sr/^{86}Sr$ ratios range from 0.710042 to 0.712843. The $^{87}Sr/^{86}Sr$ ratio of the Cévennes baryte sample hosted in the Middle Jurassic has a mid-range value of 0.710457. For the $\delta^{34}S$ signature, there is no clear correlation between baryte and the host-rock or district. For example, in the Grands-Causses, $\delta^{34}S$ values vary from +14.0 to +23.8 ‰, between +20.0 and + 23.8 ‰ in the basement, between +14.0 and + 23.3 ‰ in the Lower Jurassic and stand at +16.9 ‰ in the Middle Jurassic. These Brt4-baryte isotopic values are consistent with those obtained previously (Aquilina et al., 2011; Fontes and Matray, 1993; Gigoux, 2015; Laurent et al., 2020; Leach et al., 2006; Sizaret et al., 2009) and reported in Fig. 5a-b.

5. Discussion

5.1. Interpretation of fluid inclusions data from the Vendée Coast deposits

Homogenization temperatures (T_h) obtained on all FIs contained in fluorite, baryte and quartz crystals range from 110.4 to 394.1 °C (Table 1; Fig. 4). These T_h values are well above the 60 °C in the Vendée Variscan basement proposed by François et al. (2020) based on low-temperature thermochronology (LTT) models. Maximum T_h are lower than the 440 °C corresponding to the boiling temperature in the H_2O-NaCl system for a salinity of 10 wt% eq. NaCl and a pressure of 390 bars (corresponding to a depth of 1.3 km according to François et al., 2020) based on simulations by Driesner and Heinrich (2007), which is coherent with observations of biphasic FIs (no demixing).

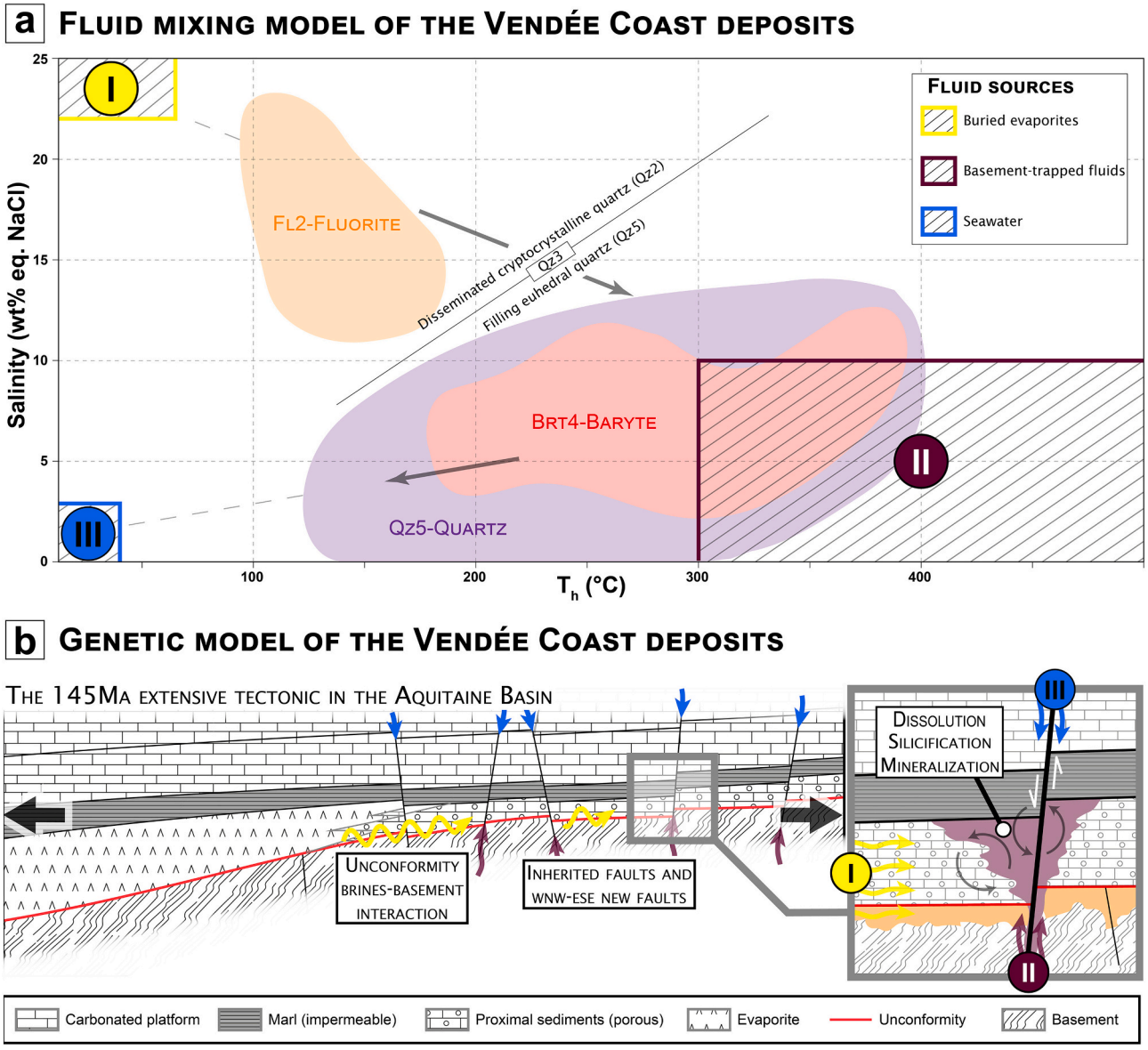

Fig. 6. a. Fluid mixing model of the Vendée Coast deposits based on mineralogy and microthermometry data of the Anse de St-Nicolas zone (Table 1; Fig. 4a). The three sources of fluids are represented by striped box and numbered as the interpreted order of appearance (see text for details). b. Genetic model of the unconformity-related deposits of the Vendée Coast in a cross-section through the Aquitaine Basin. Yellow arrows represent brines flowing from buried evaporites along the unconformity in porous sediments confined by an impermeable layer above. The brines could leach the basement along the unconformity (orange area). The fluid from the basement (purple arrows) ascends along active faults during the extensional tectonic activity (black arrows) around 145 Ma up to the unconformity. The mixing with the brines enable mineral precipitation and dissolution of the hosted sediments (light purple area). Finally, seawater (blue arrows) percolates from the surface in the hydrothermal system and mix with other fluids. (For interpretation of the references to colour in this figure legend, the reader is referred to the web version of this article.)

The paragenetic sequence (Fig. 2) shows the evolution of minerals through time and their relationship with the host rock. In Anse de St-Nicolas minerals are first disseminated in SU2-unit (stage 1 and 2), then in the basement, and finally in SU2 and SU5-units where fluorite-baryte and quartz-pyrite associations fill fractures and karsts (stage 4 to 5 respectively). As the formation temperature of the host minerals is close to that of the T_h of the FIs in unconformity-related ore deposits (Cathelineau et al., 2012), we will consider them identical in the following discussion. FIs for stage 2 fluorite, stage 4 baryte and stage 5 quartz show variations in salinity and T_h during successive mineral precipitation.

Stage 2 mineral growth at Anse de St-Nicolas is associated with relatively low temperature (T_h between 110.4 °C and 173.1 °C) and high salinity (13.3 to 21.2 wt% eq. NaCl; Table 1; Fig. 4a and Fig. 6) fluid circulation. Stages 4 and 5 are associated with a fluid salinity of between 1.0 and 12.9 wt% eq. NaCl and temperatures of 140.9 °C to 384.8 °C (Fig. 4a). Overall, during quartz growth in stage 5, there is a joint decrease in salinity from 10 to 3 wt% eq. NaCl and in temperature from 350 to 400 °C to 140 °C (Fig. 3i-j, Fig. 4a and Fig. 6).

Mineral growth at stage 5 in the Mine des Sards, Anse aux Moines and Cayola Bay shows the same trend as that described for Anse de St-Nicolas (Table 1; Fig. 4 and Fig. 6) with, however, for stage 5 in Mine des Sards, a salinity starting at 14 wt% eq. NaCl (Fig. 4a-b). This suggests that the starting fluid in the Mine des Sards at stage 2 probably has higher salinity and lower temperatures than in Anse de St-Nicolas (Fig. 4a-b and Fig. 6). The microthermometric data for the Vendée Coast deposits show a trend of decreasing salinity associated with increasing temperature path, ending with cooling to about 140 °C (Fig. 6). Mine des Sards and Anse de St-Nicolas recorded the most complete salinity-temperature path, while Anse aux Moines and Cayola Bay only recorded the end.

Analysis of the FIs allows us to establish the fluids succession of within the paragenetic sequence (Fig. 6) as follow:

(1) Circulation of low temperature brines with salinities up to 22 wt % eq. NaCl (Babel and Schreiber, 2014) probably sourced from the leaching of evaporites buried in the basin.
(2) Around 145 Ma, rise of a hot fluid through the basement faults (Bouat et al., 2023). In Vendée, no magmatic activity being described at 145 Ma, this eliminates a magmatic source for the hot fluid. Some authors have invoked an abnormally high regional geothermal gradient (Boiron et al., 2002) or the expulsion of a deep hot fluid in thermal disequilibrium with the basement. The first hypothesis is contradicted by the regional context in Vendée and neighboring regions which are affected by a normal geothermal gradient (Barbarand et al., 2001, 2013, 2020; François et al., 2020). The hypothesis of hot fluids ($T >$ 300 °C) released from the basement at 145 Ma therefore seems more probable. Previous works on the southern Armorican Massif have identified surface fluids trapped in the crust during the Variscan orogeny (Dusséaux et al., 2019, 2022; Le Hébel et al., 2007). Such a long-residence time of a surface fluids trapped in the basement- (Bons et al., 2014; Bons and Gomez-Rivas, 2020), could allow its heating then, its release into the overlying cover using inherited Variscan faults reactivated at 145 Ma.
(3) Seawater percolation along faults (Fig. 6) with low salinity (probably lower than 5 wt% eq. NaCl) and surface temperature (maximum 40 °C) as already mentioned by Cathelineau et al. (2012) from C and O isotopic analysis of calcite (last mineral of the paragenesis).

These three fluids are probably mixed sequentially during basement faults activities (Bouat et al., 2023). This is in good agreement with previous studies showing a mixing of three fluids leading to the hydrothermal deposits of the Vendée Coast (Cathelineau et al., 2012), although giving higher maximum temperatures (Fig. 4).

5.2. Sources of baryte from the Vendée Coast deposits

5.2.1. Source of strontium and barium

The $^{87}Sr/^{86}Sr$ ratios of the Vendée deposits are all higher than those of seawater or Triassic and Jurassic evaporites, which have isotopic ratios between 0.707 and 0.708 (Koepnick et al., 1990). This implies an enriched (i.e. radiogenic) source of Sr for these deposits. Basement rocks generally have a high $^{87}Sr/^{86}Sr$ ratio due to Rb-rich minerals whose radiogenic ^{87}Rb decays to ^{87}Sr (Canals and Cardellach, 1993; Valenza et al., 2000). The enrichment observed in baryte in SU5 at about 0.709581 and 0.710900 in the basement, could be explained by a significant addition of radiogenic ^{87}Sr (Table 1; Fig. 5a). In the Vendée Coast and Poitou High deposits, basement feldspars and micas are altered beneath the unconformity (Boiron et al., 2002; Cathelineau et al., 2012; Fourcade et al., 2002; Strzerzynski et al., 2020), and are known to be a possible source of radiogenic ^{87}Sr (McNutt et al., 1990). We therefore propose that the basement is the source not only of the barium but also very likely of the associated base metals, F and Si observed in the deposits of the Vendée Coast.

5.2.2. Source of sulfur

Sulfur isotopes ($\delta^{34}S$) on baryte and pyrite from the Vendée Coast vary between +23.5 and + 43.6 ‰ and between −23.5 and − 7.3 ‰, respectively (Table 1; Fig. 5a-b). This enriched signature in baryte does not correspond to a magmatic signature (around 0 ‰), which is consistent with the absence of magmatic activity at this time. Sediments, in particular evaporites which consist of sulfates minerals could be the source of sulfur in the area. In France, evaporite deposits are known from Upper Triassic to Lower Jurassic (Curnelle and Dubois, 1986; Biteau et al., 2006) with $\delta^{34}S$ signature ranging from +12 to +21 ‰ (Crockford et al., 2019; Kampschulte and Strauss, 2004). Baryte values from the Vendée Coast are higher, implying a mechanism allowing an isotopic enrichment in the $\delta^{34}S$ value. Baryte and pyrite are observed in two samples from SU2 and SU5 (Samples Pt201 and MR201, Table 1) with similar isotopic fractionations between them with a $\Delta^{34}S$ around −50 ‰. Using the fractionation equations between aqueous SO_4^{2-} and H_2S (after Eldridge et al., 2016), we obtained a temperature of 70 °C which is far below the temperature obtained by microthermometry on baryte (T_h between 195 °C 380 °C; Table 1). We concluded that sulfate-sulfide isotopic equilibrium was not been achieved in the samples from the Vendée Coast. Sulfate-sulfide disequilibrium is common in a context of low sulfidation (Hutchison et al., 2020), or as in sulfides from modern seafloor hydrothermal vent (Ono et al., 2007). Indeed, the rate of precipitation is faster than the rate of isotope exchange to reach isotopic equilibrium between aqueous sulfate and H_2S, especially during fluid mixing (Shelton and Rye, 1982; Zheng, 1991; Ohmoto and Lasaga, 1982). Baryte - which is slightly soluble (Djamali et al., 2016) - precipitate rapidly compared to pyrite, thus explaining the difficulty for this system to reach isotopic equilibrium.

In our case, the coexistence of baryte and pyrite, in such a hydrothermal context, may be due to a sulfate reduction process caused by bacterial (Bacterial Sulfate Reduction, BSR; Machel, 2001) or abiotic activities (Thermochemical Sulfate Reduction, TSR; Goldstein and Aizenshtat, 1994). BSR is ineffective above 80 °C, as sulfate-reducing bacteria cease to metabolize (Machel, 2001). In contrast, TSR is effective above 120 °C (Goldstein and Aizenshtat, 1994; Machel, 2001). Temperatures obtained on baryte FIs from of the Vendée Coast are >150 °C, suggesting that TSR is the more likely process to explain the co-precipitation of baryte and pyrite. The catalyst for TSR is a reducing agent which may be organic matter, potentially present either in the sediments (Galbrun et al., 1994) or in the basement (Le Corre et al., 1991; Le Hébel et al., 2007).

North of the Aquitaine Basin, the largest source of sulfur in the Lower Jurassic sediments is the Hettangian Anhydrite Zone (Biteau et al., 2006; Curnelle and Dubois, 1986), whose $\delta^{34}S$ signature is +14.2 ‰ (Crockford et al., 2019). To explain the significant enrichment of some

baryte compared to Lower Jurassic anhydrites, we performed Rayleigh distillation calculations (e.g., Seal, 2006). The observed isotopic signature could result from a partial reduction of about 28 % in aqueous sulfates derived from the Lower Jurassic anhydrites for the pair hosted by SU2-unit and 58 % for the pair hosted by SU5-unit. We interpret this phenomenon as simultaneous precipitation during tectonic fracturing that extended from basement to cover. Sulfates-rich fluids derived from Lower Jurassic anhydrites probably circulated along the unconformity and mixed in the SU2-unit with ascending hot fluids (>150 °C), rich in base metals trapped in the basement, resulting in a ~ 28 % TSR reduction of the aqueous sulfates. Residual dissolved sulfates continue to be reduced by up to 58 % during fracture propagation in the Middle Jurassic formation (SU5).

Using sulfur isotopes ($\delta^{34}S$) on baryte and pyrite it is deduced that the Vendée hydrothermal system sulfur is compatible with and may originate from the Lower Jurassic Anhydrite Zone of the Aquitaine Basin, with partial reduction of aqueous sulfates by TSR.

5.3. French unconformity-related ore deposits link with brines

5.3.1. Role of buried evaporites involvement in brines formation

In this section, we will highlight the role of buried evaporites in the formation of the unconformity-related french deposits based on our data, together with data from the literature (Tables 1 and 2; Fig. 1 and Fig. 8). Quartz FIs of from the Poitou High and Albigeois districts (Massif Central) yield T_h values of 100 to 160 °C and 85 to 170 °C and salinity of 10 to 21 wt% eq. NaCl and 20–26 wt% eq. NaCl (Table 2; Fig. 7; Cathelineau et al., 2012; Munoz et al., 1999). In the southeast of the Massif Central, in the Cévennes, the T_h of the FIs of the Largentière and Trèves deposits are below 200 °C with salinities between 10 and 25 wt% eq. NaCl (Léost et al., 1999; Sabouraud et al., 1980). At Trèves, the $\delta^{34}S$ of baryte varies from +12.2 ‰ to +19.2 ‰ (Table 2; Fig. 5b; Leach et al., 2006). In Largentière, baryte data vary from +6.8 to +24.7 ‰ (Table 2; Fig. 5a, Aquilina et al., 2011). To explain these variations, the authors conclude that there is a mixture between a brine from Paleozoic-Triassic sulfates and seawater. In the Lodève district, the $\delta^{34}S$ of the baryte varies little between +15.6 and + 18.5 ‰ and the T_h varies from 50 °C to 220 °C for salinities between 1 and 21 wt% eq. NaCl (Table 2; Fig. 5a; Laurent et al., 2017, 2020).

North of the Massif Central, in the Chaillac deposit, fluorite FIs yield T_h below 150 °C and salinity of 10 to 25 wt% eq. NaCl (Fig. 7; Sizaret et al., 2004). The $\delta^{34}S$ of the baryte ranges from +13.9 ‰ to +21.0 ‰ (Table 2; Fig. 5a; Sizaret et al., 2009). In the Morvan district, Gigoux et al. (2016) obtained a lower homogenization temperature (70–140 °C) and salinities up to 16.3 wt% eq. $CaCl_2$ from FIs from the Courcelles deposit. Values of the $\delta^{34}S$ on baryte are homogeneous between +17 and + 18.5 ‰ (Table 2; Fig. 5b; Gigoux, 2015).

In all basins around the Massif Central, low-temperatures and high salinity brines showing $\delta^{34}S$ values on baryte between +12 to +21 ‰, are consistent with buried evaporites from the Upper Triassic to Lower Jurassic (Fig. 5a; Kampschulte and Strauss, 2004). These evaporites present in all these basins (Fig. 8; Biteau et al., 2006; Curnelle and Dubois, 1986; Mégnien et al., 1980) are similar to the Vendée Coast deposits reinforcing the hypothesis that here the brines likely originate from similar buried evaporites corresponding to the main sulfur stock in all these deposits. Moreover, the $\delta^{34}S$ enrichment of the baryte in these basins, can also be explained by Rayleigh distillation as in the Vendée Coast deposits.

This may imply brines transfer along the unconformity, but over a length of a few kilometers for the Morvan and Cévennes districts and at least a hundred kilometers for the Grands-Causses and Albigeois districts. This mechanism of brine expulsion by leaching from buried-evaporites is already known from the Poitou High and Cévennes deposits (Boiron et al., 2002; Cathelineau et al., 2012; Ramboz and Charef, 1988) and from the Pine Point deposits in Canada (Rhodes et al., 1984).

5.3.2. Basement-brines interactions as a source for metals

In addition to very similar mineral associations (Cathelineau et al., 2012; Gigoux et al., 2016; Laurent et al., 2017; Leach et al., 2006; Sizaret et al., 2004) and evidence of evaporitic brines circulation, all these unconformity-related deposits give arguments in favor of silicification of the cover. Moreover, the high $^{87}Sr/^{86}Sr$ ratio between 0.707 and 0.708 is higher than that of evaporites (Koepnick et al., 1990), confirming the significant influence of basement derived fluids. In the western Massif Central, Coiteux (1983) reports silicification of sediments above the unconformity in the Melle deposit (Poitou High; Fig. 1a). This phenomenon is also reported in the Périgord (Guillot et al., 1979) and Grands-Causses districts (Legendre et al., 2009; Roig et al., 2001). Furthermore, in these deposits the $^{87}Sr/^{86}Sr$ ratio on baryte range between 0.708969 (Neuil zone, Périgord district) and 0.712843 (Barjac zone, Grands-Causses disctrict). In the Albigeois district, silicification is not reported in sediments but in the fault zones (Munoz et al., 1999). To the southeast of the Massif Central, the Cévennes district host silicified sediments (Leach et al., 2006) with a wider range of $^{87}Sr/^{86}Sr$ ratios on baryte (Table 2; Fig. 5a; Aquilina et al., 2011). In Laurent et al. (2020) the $^{87}Sr/^{86}Sr$ ratio on baryte from the Lodève deposit is similar to that of the other deposits, with no silicification reported in the cover despite the propagation of silicification in fault zones as in the Albigeois district. In the northern Massif Central, sediment silicification is known as “sinter” in the Chaillac deposit (Sizaret et al., 2009) associated with baryte with an $^{87}Sr/^{86}Sr$ ratio comparable to the Lodève deposits (Table 2; Fig. 5a). In the Morvan district, pervasive silicification of sediments above the unconformity is described by Gigoux et al. (2016) in association with hydrothermal mineralizations.

All these data are consistent with brines-rock interactions between the Variscan basement and the sedimentary cover similar to that of the Vendée Coast deposits (see section 5.2.1). Alteration of feldspar and mica in these unconformity-related deposits is probably responsible for the high $^{87}Sr/^{86}Sr$ ratios, as well as high silica, base metals and F-Ba contents (Boiron et al., 2010; Burisch et al., 2016; Fourcade et al., 2002; Walter et al., 2019). Brines have the ability to leach cations from the basement and transport them via chloride complexes (Helgeson, 1964; Yardley, 2005). This could explain the similarity between Fl-Brt-Qz parageneses and sulfides associations with silicification in all these unconformity-related deposits (Table 1 and Table 2). Moreover, these different ranges of high $^{87}Sr/^{86}Sr$ ratios could be related to the diversity of lithologies in the basement from each district, or to different degree of mixing between the brines and basement-derived fluids.

5.4. French unconformity-related deposits and rifting settings with deep hot fluids

In order to establish the temporal specificity of the formation of French unconformity-related deposits, we will compare our results (Table 1) with available data on deposits emplaced in all Mesozoic basins of France (Table 2).

5.4.1. Bay of Biscay rifting

On the Vendée coast, previous studies have highlighted the link between mineral deposits and a regional N-S extension dated at 144.1 ± 26.2 Ma and characterized by NW-SE normal faults and fractures (Fig. 8, Bouat et al., 2023; Strzerzynski et al., 2020). Microthermometric data obtained on Brt4-baryte and Qz5-quartz FIs attest to the circulation of a low salinity (< 10 wt% eq. NaCl), high temperature (T° > 350 °C) fluid from the basement into these deposits (see section 5.1; Fig. 7). From Poitou High (Boiron et al., 2002) to Grand-Causses (Briand et al., 1979, 1993; Burg et al., 1992; Legendre et al., 2009; Mennessier and Collomb, 1986; Roig et al., 2001), via Périgord districts (Guillot et al., 1979), similar NW-SE trending vein deposits are observed. Further south, in the Albigeois, these are striking E-W (Munoz et al., 1999, 2005). The timing of mineral deposition is constrained between 191 Ma and 132 Ma by K—Ar and $^{40}Ar/^{39}Ar$ dating on adularia and associated clays (Table 2

Table 2
Literature data on French unconformity-related deposits reporting geological contexts, ages of the ore deposits, temperatures and salinities determined in FIs of different hosted-minerals and $^{87}Sr/^{86}Sr$-$\delta^{34}S$ on baryte (See references for details). Qz: quartz, Brt: baryte, Fl: fluorite, Mrc: marcasite, Gn: galena, Sp: sphalerite, Cal: calcite, Anh: anhydrite, Dol: dolomite.

District	Zone	Main minerals	Host-rock	Morphology	Age (Ma)	Microthermometry			Baryte		Reference
						Host	Temperature (°C)	Salinity (wt %NaCl)	$^{87}Sr/^{86}Sr$	$\delta^{34}S$ (vCDT ‰)	
Vendée Coast	Anse de St-Nicolas	Brt-Qtz-Cal	SU5-unit	NW-SE vein	144.1 ± 26.2 Ma						Bouat et al. (2023)
Poitou High	Melle	Qtz-Gn	Dolomitized arenite (Low. Jurassic)	Karst		Qtz	100–160	10–21			Cathelineau et al. (2012)
	Charroux-Civray	Qtz-Fl-Brt	Granitoid	NW-SE vein	140.5–154.3 (K—Ar & Ar—Ar)						Cathelineau et al. (2012)
	Chaillac	Fl-Brt-Gn	Micaschists and Sandstones (Low. Jurassic)	Stratiform, NNE-SSW vein	201–199 (stratigraphic)	Fl	84–150	0.4–21.8			Sizaret et al. (2004)
					154.5 (K—Ar)						Cathelineau et al. (2012)
									0.70903–0.71185	13.9–21.0	Sizaret et al. (2009)
Morvan	Pierre-Perthuis	Fl-Brt-Qtz	Silicified dolomite (Up. Triassic)	Karst	130 ± 15 (Sm—Nd)						Gigoux et al. (2015)
						Fl	76–245	1.2–10.7			Gigoux et al. (2016)
										17.5–18.3	Gigoux (2015)
	Courcelles	Fl-Brt-Qtz	Limestone (Low. Jurassic)	Stratiform		Fl	72–137	0.2–1.9			Gigoux et al. (2016)
										18.4–18.5	Gigoux (2015)
	Antully	Fl-Brt-Qtz	Sandstone (Mid. Triassic)	Stratiform		Fl	71–278	1.6–16.3 ($CaCl_2$)			Gigoux et al. (2016)
										17.0	Gigoux (2015)
	Voltennes	Fl	Rhyodacitic tuffs	NNW-SSE veins	172.5–178.3 (K—Ar)						Baubron et al. (1980) and Joseph et al. (1973) from Gigoux et al. (2015)
Grands-Causses	St-Geniez d'Olt	Brt	Micaschists	NW-SE vein	191–146 (K—Ar)						Bonhomme et al. (1987)
	Bestex	Brt	Granit	NW-SE vein	169–146 (K—Ar)						Bonhomme et al. (1987)
	Montpestels	Brt	Granit	NW-SE vein	163–149 (K—Ar)						Bonhomme et al. (1987)
	Colombiès	Brt	Micaschists	NW-SE vein	132 (K—Ar)						Bonhomme et al. (1987)
Cévennes	Largentière	Sl-Gn-Brt ± Anh ± Dol	Sandstone (Up. Triassic)	Stratiform, NE-SW vein	217–210 (K—Ar)						Bonhomme et al. (1987)
						Anh-Dol-Qtz	63–295	1–24			Léost et al. (1999)
									0.708201–0.71561	6.8–24.7	Aquilina et al. (2011)
	Masdieu	Brt	Sandstone and dolomite (Low.-Mid. Triassic)	Stratifom	213–205 (K—Ar)						Bonhomme et al. (1987)
	Trèves	Sl-Gn-Qtz ± Brt	Dolomitized carbonates (Low. Jurassic)	Stratiform, NNE-SSW vein		Qtz	60–130	15–24			Sabouraud et al. (1980)
										12.2–19.2	Leach et al. (2006)
	Gatuzières	Gn	Sandstone and carbonates (Triassic-Low. Jurassic)	NW-SE vein	188 (K—Ar)						Bonhomme et al. (1987)
	Malines	Sl-Gn-Brt ± Qtz	Cambrian dololimestones, Triassic shales and Middle Jurassic limestones	Karsts, ENE-WSW vein	271–211 (K—Ar)						Bonhomme et al. (1987)
						Brt	130–380	3–12			Ramboz and Charef (1988)
Lodève		Qtz-Brt ± Sl	Detritic sediments (Permian)	ENE-WSW vein	182–174 (K—Ar)						Bonhomme et al. (1987)
						Brt	75–222	1.7–21			Laurent et al. (2017)
						Brt	48–195	12.6–13.6	0.70888–0.711913	15.6–18.5	Laurent et al. (2020)
Albigeois	Mont-Roc	Fl-Qtz	Detritic sediments (Cambrian-Ordovician)	E-W vein	246–149 (K—Ar)						Bonhomme et al. (1987)
					111 ± 13 (Sm—Nd)						Munoz et al. (2005)
						Qtz	85–170	20.0–26.0			Munoz et al. (1999)

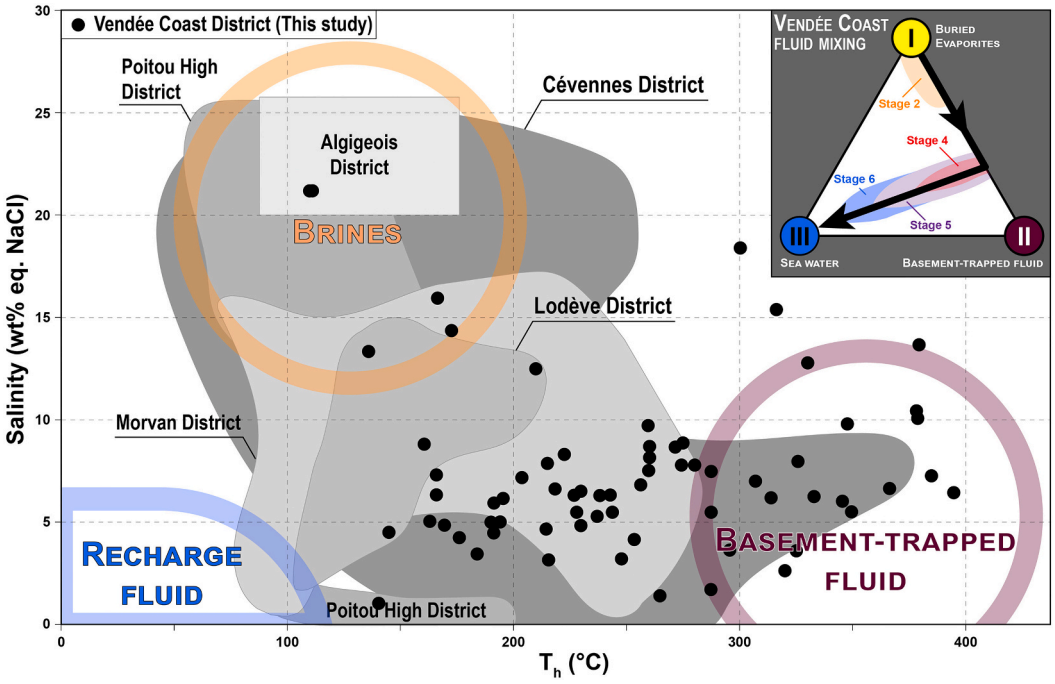

Fig. 7. Salinity-Temperature diagram of FIs from ore deposits in French basin (See Table 2 for references).

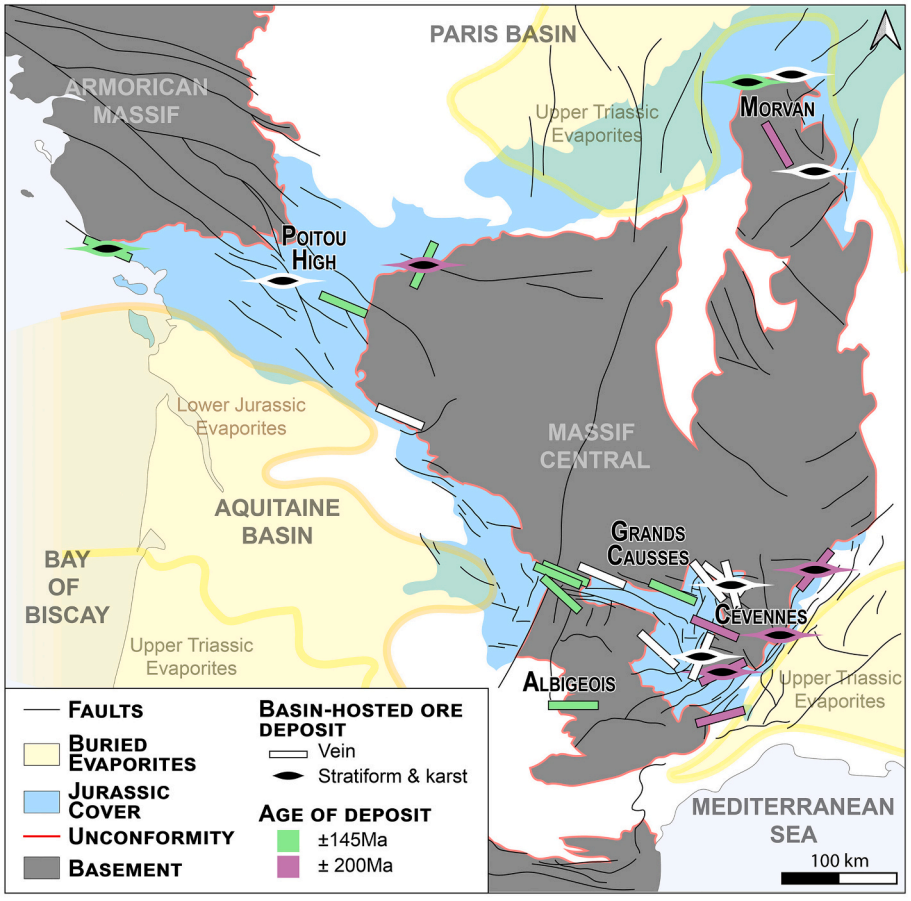

Fig. 8. Simplified geological map of France with basin-hosted ore deposits. See Table 2 for details and references about deposits age. The Upper Triassic and Lower Jurassic map of the buried evaporites from Curnelle and Dubois (1986) and Mégnien et al. (1980).

and Fig. 8; Bonhomme et al., 1987, Cathelineau et al., 2012) and Sm—Nd dating on fluorite (Munoz et al., 2005). This wide age range is related to alteration processes over a long period of time but also to the presence of a fraction of white micas inherited from the older Variscan basement (Bonhomme et al., 1987; Cathelineau et al., 2012). We consider that the mineralized deposits were probably formed in the youngest part of these periods obtained for each deposit, i.e. around 155 and 140 Ma in the Poitou High (Table 2 and Fig. 8; Cathelineau et al., 2012) and around 149 Ma and 111 Ma in the Grands-Causses and Albigeois, respectively (Bonhomme et al., 1987; Munoz et al., 2005). West of the Massif Central, in the region including Vendée Coast, Poitou High, Périgord and Grands-Causses districts, unconformity-related deposits formed between the Upper Jurassic and the Lower Cretaceous. Their veins oriented NW-SE (Fig. 8) are consistent with the onset of rifting in the Bay of Biscay (Asti et al., 2022; Bouat et al., 2023; Constantin et al., 2002; Jammes et al., 2009), located west of the Variscan Massifs (Fig. 8). So, the rifting in the Bay of Biscay probably control the formation of the unconformity-related deposits located from the Vendée Coast to the Grands-Causses.

5.4.2. *Alpine Tethys rifting*

In the Cévennes (Alabouvette et al., 1988; Aquilina et al., 2011; Leach et al., 2006) and Lodève districts (Laurent et al., 2017), the veins show a more complex NNE-SSW to NE-SW orientation. Chronological data obtained on these veins range from 211 Ma to 174 Ma (Bonhomme et al., 1987). Microthermometric analyses of Les Malines baryte FIs by Ramboz and Charef (1988) indicate that these deposits are related to the circulation of a fluid of low salinity (<10 wt% eq. NaCl, Table 2; Fig. 7) and high temperature (up to 380 °C). In the same district, Léost et al. (1999) report a maximum fluid temperature of 295 °C with a salinity of <5 wt% eq. NaCl (Table 2).

Based on these results, we propose a model for ore deposits genesis that involves the ascent of deep hot fluids from the basement in an extensional context. The stress field and the ages of the deposits may vary locally. For example, the deposits of the southeastern Massif Central are dated from the Upper Triassic to the Lower Jurassic with the same NE-SW strike. However, at that time, the southeast Massif Central correspond to the western margin of the Alpine Tethys (Handy et al., 2010; Lemoine et al., 1986; Stampfli and Borel, 2002). Therefore, this rifting appears to control the Cévennes and Lodève basin-hosted ore deposits (Fig. 8). Thus, the southeast Massif Central unconformity-related deposits seem to form in the context of the rifting of the Alpine Tethys.

5.4.3. *Multi-phase unconformity-related ore deposits*

On the northern side of the Massif Central, the deposits are both stratiform in the sedimentary cover and in basement faults oriented NNE-SSW (Chaillac deposit; Sizaret et al., 2004) or NNW-SSE (Morvan district; Gigoux et al.,2015). In the Morvan district, basement-hosted fluorite deposits are dated to the Lower Jurassic (K—Ar on adularia; Gigoux et al., 2015; after Baubron et al., 1980 and Joseph et al., 1973) and to the Lower Cretaceous in the sedimentary cover (Sm—Nd on fluorite, Table 2 and Fig. 8; Gigoux et al., 2015). Preliminary results on U—Pb fluorite overgrowths yield ~40 Ma (Lenoir et al., 2021). At Chaillac, the deposits are dated indirectly to the Lower Jurassic by Sizaret et al. (2004) and to 155 Ma (K—Ar dating on adularia) by Cathelineau et al. (2012).

Gigoux et al. (2016) and Sizaret et al. (2004) have shown that the Morvan and Chaillac deposits were formed at relatively low temperatures. In the Antully fluorite deposits from Morvan, the temperature of the fluid ranges between 70 and 280 °C (Table 2; Fig. 7; Gigoux et al., 2016). Similarities between deposits on the Vendée Coast and Antully deposits could suggest the involvement of a basement-derived fluid for the later but further field investigations are required. These previous works highlight at least two mineralizing stages.

Our work on the ore deposits of the Vendée Coast complements previous studies on deposits on a European scale (Muchez et al., 2005), demonstrating that the formation of base metals deposits is likely favored in a context of intracontinental rifting. In such a context, faults crossing the unconformity could allow significant fluids-rocks interactions involving brines or, in some cases, the potential release of trapped fluids in the basement, as in the Vendée Coast district and Les Malines deposits (Ramboz and Charef, 1988). In France, Mesozoic rifting took place in two major stages: the opening of the Bay of Biscay and the Tethys Rift. Both periods seem to be associated with at least two stages of mineralizations at the Triassic-Jurassic transition in the southeast of the Massif Central, and at the Jurassic-Cretaceous transition in the southwest and the west of the Massif Central.

6. Conclusion

On the Vendée Coast, petrographic observations coupled with the analysis of FIs allowed to propose the succession of three different fluids responsible for the formation of the deposits: i) brines deriving from the leaching of evaporites buried in the basin, ii) hot fluids rising from the basement and iii) the incursion of seawater from the surface. Isotopic data for baryte from the deposits on the Vendée Coast and French unconformity deposits seem to indicate fluids-rocks interactions involving sulfur-rich brines altering basement feldspars and micas the along the unconformity.

On a global scale we show that in western Europe, brines originating from the leaching of buried evaporites could be at the origin of the formation of all unconformity-related deposits. Our study makes it possible to define the structural framework of the formation of these deposits. The prevailing extensional context corresponds to two successive stages of rifting: i) the rifting of the Alpine Tethys (southeast of the Massif Central) and the rifting of the Bay of Biscay (west of the Variscan massifs). Finally, our study open news opportunities for the exploration of such deposits. By combining a precise structural and microstructural study coupled with the analysis of fluids and their source, could lead to a better targeting of unconformity-related deposits.

Supplementary data to this article can be found online at https://doi.org/10.1016/j.gexplo.2025.107713.

CRediT authorship contribution statement

Loïc Bouat: Writing – original draft, Visualization, Supervision, Methodology, Investigation, Conceptualization. **Pierre Strzerzynski:** Writing – original draft, Visualization, Supervision, Methodology, Investigation, Conceptualization. **Véronique Gardien:** Writing – original draft, Methodology, Investigation. **Guillaume Barré:** Writing – original draft, Methodology, Investigation. **Yannick Branquet:** Writing – original draft, Methodology, Investigation. **Jérémie Melleton:** Writing – original draft, Investigation. **Régis Mourgues:** Conceptualization.

Declaration of competing interest

The authors declare the following financial interests/personal relationships which may be considered as potential competing interests: Strzerzynski reports financial support was provided by National Centre for Scientific Research. Strzerzynski reports financial support was provided by Nantes Atlantic Observatory of the Sciences of the Universe. If there are other authors, they declare that they have no known competing financial interests or personal relationships that could have appeared to influence the work reported in this paper.

Acknowledgements

This work was founded by the Tellus-Cessur program of CNRS and by the OSUNA (France). The authors are grateful of Laurent Lenta from Laboratoire de Planétologie et Géodynamique for sample preparation,

David Vilbert from Géosciences Rennes for the $^{87}Sr/^{86}Sr$ isotopic ratio analysis of baryte samples and Thomas Rigaudier from CRPG for the sulfur isotopes analysis of baryte and pyrite samples presented in this study.

Data availability

All the data used in this manuscript are inserted into the text and in the supplementary materials section.

References

Alabouvette, B., Arthaud, F., Bodeur, Y., Barthes, J.-P., Paloc, H., Aubague, M., 1988. Notice explicative, Carte géol. France (1/50000), feuille Le Vigan (937) 67.

Anderson, G.M., 1975. Precipitation of Mississippi Valley-type ores. Econ. Geol. 70, 937–942. https://doi.org/10.2113/gsecongeo.70.5.937.

Aquilina, L., Boulvais, P., Mossmann, J.-R., 2011. Fluid migration at the basement/sediment interface along the margin of the Southeast basin (France): implications for Pb–Zn ore formation. Mineral. Deposita 46, 959–979. https://doi.org/10.1007/s00126-011-0360-9.

Asti, R., Saspiturry, N., Angrand, P., 2022. The Mesozoic Iberia-Eurasia diffuse plate boundary : a wide domain of distributed transtensional deformation progressively focusing along the North Pyrenean Zone. Earth Sci. Rev. 230, 104040. https://doi.org/10.1016/j.earscirev.2022.104040.

Babel, M., Schreiber, B.C., 2014. 9.17-Geochemistry of evaporites and evolution of seawater. Treatise Geochem. 483–560. https://doi.org/10.1016/B978-0-08-095975-7.00718-X.

Ballèvre, M., Bosse, V., Ducassou, C., Pitra, P., 2009. Palaeozoic history of the Armorican Massif: Models for the tectonic evolution of the suture zones. Compt. Rendus Geosci. 341, 174–201. https://doi.org/10.1016/j.crte.2008.11.009.

Barbarand, J., Lucazeau, F., Pagel, M., Séranne, M., 2001. Burial and exhumation history of the south-eastern Massif Central (France) constrained by apatite fission-track thermochronology. Tectonophysics 335, 275–290. https://doi.org/10.1016/S0040-1951(01)00069-5.

Barbarand, J., Préhaud, P., Baudin, F., Missenard, Y., Matray, J.M., François, T., Blaise, T., Pinna-Jamme, R., Gautheron, C., 2020. Where are the limits of Mesozoic intracontinental sedimentary basins of southern France? Mar. Pet. Geol. 121, 104589. https://doi.org/10.1016/j.marpetgeo.2020.104589.

Barbarand, J., Quesnel, F., Pagel, M., 2013. Lower Paleogene denudation of Upper cretaceous cover of the Morvan Massif and southeastern Paris Basin (France) revealed by AFT thermochronology and constrained by stratigraphy and paleosurfaces. Tectonophysics 608, 1310–1327. https://doi.org/10.1016/j.tecto.2013.06.011.

Baubron, J.C., Jébrak, M., Joannès, C., Lhégu, J., Touray, J.C., Ziserman, A., 1980. Nouvelles datations K/Ar sur des filons à quartz et fluorine du Massif Central français. C. R. Acad. Sci. 290, 951–953.

Biteau, J.-J., Marrec, A.L., Vot, M.L., Masset, J.-M., 2006. The Aquitaine Basin. Pet. Geosci. 12, 247–273. https://doi.org/10.1144/1354-079305-674.

Blundell, D.J., Karnkowski, P.H., Alderton, D.H.M., Oszczepalski, S., Kucha, H., 2003. Copper mineralization of the Polish Kupferschiefer: a proposed basement fault-fracture system of fluid flow. Econ. Geol. 98, 1487–1495. https://doi.org/10.2113/gsecongeo.98.7.1487.

Bodnar, R.J., 1993. Revised equation and table for determining the freezing point depression of H2O-NaCl solutions. Geochim. Cosmochim. Acta U. S. 57, 3. https://doi.org/10.1016/0016-7037(93)90378-A.

Boiron, M.C., Cathelineau, M., Banks, D.A., Buschaert, S., Fourcade, S., Coulibaly, Y., Michelot, J.L., Boyce, A., 2002. Fluid transfers at a basement/cover interface Part II. Large-scale introduction of chlorine into the basement by Mesozoic basinal brines. Chem. Geol. 20.

Boiron, M.-C., Cathelineau, M., Richard, A., 2010. Fluid flows and metal deposition near basement /cover unconformity: lessons and analogies from Pb–Zn–F–Ba systems for the understanding of Proterozoic U deposits. Geofluids 10, 270–292. https://doi.org/10.1111/j.1468-8123.2010.00289.x.

Bonhomme, M.G., Baubron, J.-C., Jebrak, M., 1987. Minéralogie, géochimie, terres bares et age K Ar des argiles associées aux minéralisations filoniennes. Chem. Geol. Isot. Geosci. Sect. 65, 321–339. https://doi.org/10.1016/0168-9622(87)90012-1.

Bons, P.D., 2001. The formation of large quartz veins by rapid ascent of fluids in mobile hydrofractures. Tectonophysics 336, 1–17. https://doi.org/10.1016/S0040-1951(01)00090-7.

Bons, P.D., Fusswinkel, T., Gomez-Rivas, E., Markl, G., Wagner, T., Walter, B., 2014. Fluid mixing from below in unconformity-related hydrothermal ore deposits. Geology 42, 1035–1038. https://doi.org/10.1130/G35708.1.

Bons, P.D., Gomez-Rivas, E., 2020. Origin of Meteoric Fluids in Extensional Detachments. Geofluids 2020, e7201545. https://doi.org/10.1155/2020/7201545.

Bouat, L., Strzerzynski, P., Mourgues, R., Branquet, Y., Cogné, Y., Barré, G., Gardien, V., 2023. Early, far-field and diffuse tectonics records in the North Aquitaine Basin (France). BSGF-Earth Sciences Bulletin 194, 17. https://doi.org/10.1051/bsgf/2023014.

Briand, B., Combémorel, R., Couturié, J.-P., Bérard, P., Vautrelle, C., 1993. Notice explicative, Carte géol. France (1/50000), feuille Le Bleymard (863) 73.

Briand, B.-G., Couturié, J.-P., Geffroy, J., Gèze, B., 1979. Notice explicative, Carte géol. France (1/50000), feuille Mende (862) 192.

Brunet, M.-F., 1984. Subsidence history of the Aquitaine basin determined from subsidence curves. Geol. Mag. 121, 421–428. https://doi.org/10.1017/S0016756800029952.

Brunet, M.-F., Le Pichon, X., 1982. Subsidence of the Paris basin. J. Geophys. Res. Solid Earth 87, 8547–8560. https://doi.org/10.1029/JB087iB10p08547.

Burg, J.-P., Alabouvette, B., Astruc, J.G., Lefavrais-Raymond, A., Lereloup, A.F., Vautrelle, C., 1992. Notice explicative, Carte géol. France (1/50000), feuille Rieupeyroux (883) 69.

Burisch, M., Marks, M.A.W., Nowak, M., Markl, G., 2016. The effect of temperature and cataclastic deformation on the composition of upper crustal fluids — an experimental approach. Chem. Geol. 433, 24–35. https://doi.org/10.1016/j.chemgeo.2016.03.031.

Cagnard, F., Gapais, D., Brun, J.P., Gumiaux, C., Van den Driessche, J., 2004. Late pervasive crustal-scale extension in the south Armorican Hercynian belt (Vendée, France). J. Struct. Geol. 26, 435–449. https://doi.org/10.1016/j.jsg.2003.08.006.

Canals, A., Cardellach, E., 1993. Strontium and Sulphur isotope geochemistry of low-temperature barite-fluorite veins of the Catalonian Coastal Ranges (NE Spain): a fluid mixing model and age constraints. Chem. Geol. 104, 269–280. https://doi.org/10.1016/0009-2541(93)90156-D.

Cathelineau, M., Boiron, M.-C., Fourcade, S., Ruffet, G., Clauer, N., Belcourt, O., Coulibaly, Y., Banks, D.A., Guillocheau, F., 2012. A major Late Jurassic fluid event at the basin/basement unconformity in western France: 40Ar/39Ar and K–Ar dating, fluid chemistry, and related geodynamic context. Chem. Geol. 322–323, 99–120. doi:https://doi.org/10.1016/j.chemgeo.2012.06.008.

Cheilletz, A., Gasquet, D., Filali, F., Archibald, D.A., Nespolo, M., 2010. A late Triassic 40 Ar/39 Ar age for the El Hammam high-REE fluorite deposit (Morocco): mineralization related to the Central Atlantic Magmatic Province? Miner. Deposita 45, 323–329. https://doi.org/10.1007/s00126-010-0282-y.

Coiteux, S., 1983. Le Métallotecte de Melle (Deux-Sèvres), contexte sédimentaire et minéralisations (PhD dissertation).. Université de Poitiers.

Constantin, J., Vergély, P., Cabrera, J., 2002. Tectonic evolution and related fracturing in the Causses Basin (Aveyron, France) : the Tournemire area example. Bull. Société Géologique Fr. 173, 229–243. doi:https://doi.org/10.2113/173.3.229.

Corbella, M., Ayora, C., Cardellach, E., 2004. Hydrothermal mixing, carbonate dissolution and sulfide precipitation in Mississippi Valley-type deposits. Mineral. Deposita 39, 344–357. https://doi.org/10.1007/s00126-004-0412-5.

Corbella, M., Ayora, C., Cardellach, E., Soler, A., 2006. Reactive transport modeling and hydrothermal karst genesis: the example of the Rocabruna barite deposit (Eastern Pyrenees). Chem. Geol. 233, 113–125. https://doi.org/10.1016/j.chemgeo.2006.02.022.

Crockford, P.W., Kunzmann, M., Bekker, A., Hayles, J., Bao, H., Halverson, G.P., Peng, Y., Bui, T.H., Cox, G.M., Gibson, T.M., Wörndle, S., Rainbird, R., Lepland, A., Swanson-Hysell, N.L., Master, S., Sreenivas, B., Kuznetsov, A., Krupenik, V., Wing, B. A., 2019. Claypool continued: Extending the isotopic record of sedimentary sulfate. Chem. Geol. 513, 200–225. https://doi.org/10.1016/j.chemgeo.2019.02.030.

Curnelle, R., Dubois, P., 1986. Evolution mesozoique des grands bassins sedimentaires francais; bassins de Paris, d'Aquitaine et du Sud-Est. Bull. Société Géologique Fr. II, 529–546. https://doi.org/10.2113/gssgfbull.II.4.529.

Djamali, E., Chapman, W.G., Cox, K.R., 2016. A systematic investigation of the thermodynamic properties of aqueous barium sulfate up to high temperatures and high pressures. J. Chem. Eng. Data 61, 3585–3594. https://doi.org/10.1021/acs.jced.6b00506.

Driesner, T., Heinrich, C.A., 2007. The system H2O–NaCl. Part I: Correlation formulae for phase relations in temperature–pressure–composition space from 0 to 1000°C, 0 to 5000bar, and 0 to 1 XNaCl. Geochim. Cosmochim. Acta 71, 4880–4901. https://doi.org/10.1016/j.gca.2006.01.033.

Dusséaux, C., Gébelin, A., Boulvais, P., Gardien, V., Grimes, S., Mulch, A., 2019. Meteoric fluid-rock interaction in Variscan shear zones. Terra Nova 31, 366–372. https://doi.org/10.1111/ter.12392.

Dusséaux, C., Gébelin, A., Boulvais, P., Ruffet, G., Poujol, M., Cogné, N., Branquet, Y., Mottram, C., Barou, F., Mulch, A., 2022. Timing and duration of meteoric water infiltration in the Quiberon detachment zone (Armorican Massif, Variscan belt, France). J. Struct. Geol. 156, 104546. https://doi.org/10.1016/j.jsg.2022.104546.

Eldridge, D.L., Guo, W., Farquhar, J., 2016. Theoretical estimates of equilibrium sulfur isotope effects in aqueous sulfur systems: Highlighting the role of isomers in the sulfite and sulfoxylate systems. Geochim. Cosmochim. Acta 195, 171–200. https://doi.org/10.1016/j.gca.2016.09.021.

Faure, M., Lardeaux, J.-M., Ledru, P., 2009. A review of the pre-Permian geology of the Variscan French Massif Central. Compt. Rendus Geosci. 341, 202–213. https://doi.org/10.1016/j.crte.2008.12.001.

Fauré, P., Bohain, P., 2017. Les ammonites du Pliensbachien inférieur de la Vendée méridionale, France: étude taxonomique implications stratigraphiques et paléogéographiques, Strata. Strata Dédale Ed, Gaillac Lyon.

Fontes, J.Ch., Matray, J.M., 1993. Geochemistry and origin of formation brines from the Paris Basin, France: 1. Brines associated with Triassic salts. Chem. Geol. 109, 149–175. https://doi.org/10.1016/0009-2541(93)90068-T.

Fourcade, S., Michelot, J.L., Buschaert, S., Cathelineau, M., Freiberger, R., Coulibaly, Y., Aranyossy, J.F., 2002. Fluid transfers at the basement/cover interface part I. Subsurface recycling of trace carbonate from granitoid basement rocks (France). Chem. Geol. 21. https://doi.org/10.1016/S0009-2541(02)00192-4.

François, T., Barbarand, J., Wyns, R., 2020. Lower cretaceous inversion of the European Variscan basement: record from the Vendée and Limousin (France). Int. J. Earth Sci. 109, 1837–1852. https://doi.org/10.1007/s00531-020-01875-z.

Galbrun, B., Baudin, F., Bassoullet, J.-P., Depeche, F., Emmanuel, L., Lachkar, G., Renard, M., Riveline, J., Gabilly, J., Hantzpergue, P., 1994. Stratigraphie intégrée du

Toarcien stratotypique (coupes de Thouars et Airvault, Deux-Sèvres, France). Geobios 27, 575–595. https://doi.org/10.1016/S0016-6995(94)80222-X.
Garven, G., 1985. The role of regional fluid flow in the genesis of the Pine Point Deposit, Western Canada sedimentary basin. Econ. Geol. 80, 307–324. https://doi.org/10.2113/gsecongeo.80.2.307.
Gigoux, M., 2015. Origine des minéralisations stratiformes de fluorine de la bordure sud-est du bassin de Paris (PhD dissertation).. Université, Paris Sud - Paris XI.
Gigoux, M., Brigaud, B., Pagel, M., Delpech, G., Guerrot, C., Augé, T., Négrel, P., 2016. Genetic constraints on world-class carbonate- and siliciclastic-hosted stratabound fluorite deposits in Burgundy (France) inferred from mineral paragenetic sequence and fluid inclusion studies. Ore Geol. Rev. 72, 940–962. https://doi.org/10.1016/j.oregeorev.2015.09.013.
Gigoux, M., Delpech, G., Guerrot, C., Pagel, M., Augé, T., Négrel, P., Brigaud, B., 2015. Evidence for an early cretaceous mineralizing event above the basement/sediment unconformity in the intracratonic Paris Basin: paragenetic sequence and Sm-Nd dating of the world-class Pierre-Perthuis stratabound fluorite deposit. Mineral. Deposita 50, 455–463. https://doi.org/10.1007/s00126-015-0592-1.
Goujou, J.C., Debrand-Passard, S., Hantzpergue, P., Lebret, P., 1994. Notice explicative, Carte géol. France (1/50000), feuille Les Sables d'Olonne-Longeville (584) 95.
Guillot, P.-L., Floc'h, J.-P. Roger, Ph., Platel, J.P, Texier, J.-P., Raynal, J.-P., Pouchan, P., Recoing, M., 1979. Notice explicative, Carte géol. France (1/50000), feuille Thiviers (735) 60.
Goldstein, T., Aizenshtat, Z., 1994. Thermochemical sulfate reduction a review. J. Therm. Anal. Calorim. 42, 241–290. https://doi.org/10.1007/bf02547004.
Handy, M.R., Schmid, S.M., Bousquet, R., Kissling, E., Bernoulli, D., 2010. Reconciling plate-tectonic reconstructions of Alpine Tethys with the geological–geophysical record of spreading and subduction in the Alps. Earth Sci. Rev. 102, 121–158. https://doi.org/10.1016/j.earscirev.2010.06.002.
Heijlen, W., Muchez, P., Banks, D.A., Schneider, J., Kucha, H., Keppens, E., 2003. Carbonate-hosted Zn-Pb deposits in Upper Silesia, Poland: Origin and evolution of mineralizing fluids and constraints on genetic models. Econ. Geol. 98, 911–932. https://doi.org/10.2113/gsecongeo.98.5.911.
Helgeson, H.C., 1964. Complexing and hydrothermal ore deposition. International Series of Monographs on Earth. 17. https://doi.org/10.1016/C2013-0-01742-2.
Hitzman, M.W., Selley, D., Bull, S., 2010. Formation of sedimentary rock-hosted stratiform copper deposits through Earth history. Econ. Geol. 105, 627–639. https://doi.org/10.2113/gsecongeo.105.3.627.
Hutchison, W., Finch, A.A., Boyce, A.J., 2020. The sulfur isotope evolution of magmatic-hydrothermal fluids: Insights into ore-forming processes. Geochim. Cosmochim. Acta 288, 176–198. https://doi.org/10.1016/j.gca.2020.07.042.
Iglesias, M., Brun, J.-P., 1976. Signification des variations et anomalies de la déformation dans un segment de la chaîne hercynienne (les séries cristallophylliennes de la Vendée littorale, Massif armoricain). Bull. Société Géologique Fr. 7, 1443–1452. https://doi.org/10.2113/gssgfbull.S7-XVIII.6.1443.
Ingebritsen, S.E., Appold, M.S., 2012. The physical hydrogeology of ore deposits. Econ. Geol. 107, 559–584. https://doi.org/10.2113/econgeo.107.4.559.
Jammes, S., Manatschal, G., Lavier, L., Masini, E., 2009. Tectonosedimentary evolution related to extreme crustal thinning ahead of a propagating ocean: example of the western Pyrenees. Tectonics 28. https://doi.org/10.1029/2008TC002406.
Joseph, D., Bellon, H., Derre, C., Touray, J.C., 1973. Fluorite veins dated in the 200 million year range at La Petite Verrière and Chavaniac, France. Econ. Geol. 68, 707–708.
Kampschulte, A., Strauss, H., 2004. The sulfur isotopic evolution of Phanerozoic seawater based on the analysis of structurally substituted sulfate in carbonates. Chem. Geol. 204, 255–286. https://doi.org/10.1016/j.chemgeo.2003.11.013.
Koepnick, R.B., Denison, R.E., Burke, W.H., Hetherington, E.A., Dahl, D.A., 1990. Construction of the Triassic and Jurassic portion of the Phanerozoic curve of seawater 87Sr/86Sr. Chem. Geol. Isot. Geosci. Sect. 80, 327–349. https://doi.org/10.1016/0168-9622(90)90014-4.
Kyle, J.R., Li, N., 2002. Jinding: a Giant Tertiary Sandstone-Hosted Zn-Pb Deposit, Yunnan. China. SEG Discov. 1–16. https://doi.org/10.5382/SEGnews.2002-50.fea.
Laurent, D., Lopez, M., Chauvet, A., Sauvage, A.C., Buatier, M., Spangenberg, J.E., 2017. Sedimentary fluids/fault interaction during syn-rift burial of the Lodève Permian Basin (Hérault, France): an example of seismic-valve mechanism in active extensional faults. Mar. Pet. Geol. 88, 303–328. https://doi.org/10.1016/j.marpetgeo.2017.08.021.
Laurent, D., Lopez, M., Combes, P.-J., Guerrot, C., Spangenberg, J.E., Gaucher, E.C., 2020. Synsedimentary to early diagenetic rejuvenation of barite-sulfides ore deposits: example of the Triassic intrakarstic mineralization in the Lodève basin (France). Mar. Pet. Geol. 119, 104464. https://doi.org/10.1016/j.marpetgeo.2020.104464.
Lawrence, S.R., Cornford, C., 1995. Basin geofluids. Basin Res. 7, 1–7. https://doi.org/10.1111/j.1365-2117.1995.tb00090.x.
Le Corre, C., Auvray, B., Ballèvre, M., Robardet, M., 1991. Le Massif Armoricain/the Armorican Massif. Sci. Géologiques Bull. Mém. 44, 31–103.
Le Hébel, F.L., Fourcade, S., Boiron, M.-C., Cathelineau, M., Capdevila, R., Gapais, D., 2007. Fluid history during deep burial and exhumation of oil-bearing volcanics, Hercynian Belt of southern Brittany. France. Am. J. Sci. 307, 1096–1125. https://doi.org/10.2475/09.2007.03.
Leach, D., Macquar, J.-C., Lagneau, V., Leventhal, J., Emsbo, P., Premo, W., 2006. Precipitation of lead–zinc ores in the Mississippi Valley-type deposit at Trèves, Cévennes region of southern France. Geofluids 6, 24–44. https://doi.org/10.1111/j.1468-8123.2006.00126.x.
Leach, D., Sangster, D.F., Kelley, K.D., Large, R.R., Garven, G., Allen, C.R., Gutzmer, J., Walters, S., 2005. Sediment-Hosted Lead-Zinc Deposits: A Global Perspective 561–608. https://doi.org/10.5382/AV100.18.
Leach, D., Taylor, R.D., Fey, D.L., Diehl, S.F., Saltus, R.W., 2010. A Deposit Model for Mississippi Valley-Type Lead-Zinc Ores. Chapter A of mineral deposit models for resource assessment, USGS, Washington.
Ledru, P., Lardeaux, J.-M., Santallier, D., Autran, A., Quenardel, J.M., Floc'h, J.P., Lerouge, G., Maillet, N., Marchand, J., Ploquin, A., 1989. Où sont les nappes dans le Massif Central français? Bull. Société Géologique Fr. 605–618. https://doi.org/10.2113/gssgfbull.V.3.605.
Legendre, C., Briand, B., Thierry, J., Lebret, P., Joly, A., Bertin, C., Coint, N., Cotton, J., Guillou, H., 2009. Notice explicative, Carte géol. France (1/50000), feuille Saint-Geniez-d'Olt (861) 192.
Lemoine, M., Bas, T., Arnaud-Vanneau, A., Arnaud, H., Dumont, T., Gidon, M., Bourbon, M., de Graciansky, P.-C., Rudkiewicz, J.-L., Megard-Galli, J., 1986. The continental margin of the Mesozoic Tethys in the Western Alps. Mar. Pet. Geol. 3, 179–199. https://doi.org/10.1016/0264-8172(86)90044-9.
Lenoir, L., Blaise, T., Somogyi, A., Brigaud, B., Barbarand, J., Boukari, C., Nouet, J., Brézard-Oudot, A., Pagel, M., 2021. Uranium incorporation in fluorite and exploration of U–Pb dating. Geochronology 3, 199–227. doi:https://doi.org/10.5194/gchron-3-199-2021.
Léost, I., Renac, C., Ramboz, C., Bril, H., 1999. Circulations hydrothermales diachrones et regimes de pression contrastes sur la marge ardechoise de part et d'autre de la faille d'Uzer (forages de Balazuc et Morte Merie); mise en evidence par l'etude des inclusions fluides dans leur contexte petrostructural. Bull. Société Géologique Fr. 170, 379–390.
Machel, H.G., 2001. Bacterial and thermochemical sulfate reduction in diagenetic settings — old and new insights. Sediment. Geol. 140, 143–175. https://doi.org/10.1016/S0037-0738(00)00176-7.
Matte, P., 1986. Tectonics and plate tectonics model for the Variscan belt of Europe. Tectonophysics 126, 329–374. https://doi.org/10.1016/0040-1951(86)90237-4.
McNutt, R.H., Frape, S.K., Fritz, P., Jones, M.G., MacDonald, I.M., 1990. The 87Sr86Sr values of Canadian Shield brines and fracture minerals with applications to groundwater mixing, fracture history, and geochronology. Geochim. Cosmochim. Acta 54, 205–215. https://doi.org/10.1016/0016-7037(90)90208-3.
Mégnien, C., Mégnien, F., Debrand-Passard, S., 1980. Synthèse géologique du bassin de Paris. Mémoire du B.R.G.M. B.R.G.M Ed, Orléans.
Mennessier, G., Collomb, P., 1986. Notice explicative, Carte géol. France (1/50000), feuille St-Beauzély (909) 41.
Muchez, P., Heijlen, W., Banks, D., Blundell, D., Boni, M., Grandia, F., 2005. 7: Extensional tectonics and the timing and formation of basin-hosted deposits in Europe. Ore Geol. Rev. 27, 241–267. https://doi.org/10.1016/j.oregeorev.2005.07.013.
Munoz, M., Boyce, A.J., Courjault-Rade, P., Fallick, A.E., Tollon, F., 1994. Multi-stage fluid incursion in the Palaeozoic basement-hosted Saint-Salvy ore deposit (NW Montagne Noire, southern France). Appl. Geochem. 9, 609–626. https://doi.org/10.1016/0883-2927(94)90022-1.
Munoz, M., Boyce, A.J., Courjault-Rade, P., Fallick, A.E., Tollon, F., 1999. Continental basinal origin of ore fluids from southwestern Massif Central fluorite veins (Albigeois, France): evidence from fluid inclusion and stable isotope analyses. Appl. Geochem. 14, 447–458. https://doi.org/10.1016/S0883-2927(98)00070-5.
Munoz, M., Premo, W.R., Courjault-Radé, P., 2005. Sm–Nd dating of fluorite from the worldclass Montroc fluorite deposit, southern Massif Central. France. Miner. Deposita 39, 970–975. https://doi.org/10.1007/s00126-004-0453-9.
Ohmoto, H., Lasaga, A.C., 1982. Kinetics of reactions between aqueous sulfates and sulfides in hydrothermal systems. Geochim. Cosmochim. Acta 46, 1727–1745. https://doi.org/10.1016/0016-7037(82)90113-2.
Oliver, N.H., McLellan, J.G., Hobbs, B.E., Cleverly, J.S., Ord, A., Feltrin, L., 2006. Numerical models of extensional deformation, heat transfer, and fluid flow across basement-cover interfaces during basin-related mineralization. Econ. Geol. 101, 1–31. https://doi.org/10.2113/gsecongeo.101.1.1.
Ono, S., Shanks III, W.C., Rouxel, O.J., Rumble, D., 2007. S-33 constraints on the seawater sulfate contribution in modern seafloor hydrothermal vent sulfides. Geochim. Cosmochim. Acta 71, 1170–1182. https://doi.org/10.1016/j.gca.2006.11.017.
Ortiz, A., Guillocheau, F., Lasseur, E., Briais, J., Robin, C., Serrano, O., Fillon, C., 2020. Sediment routing system and sink preservation during the post-orogenic evolution of a retro-foreland basin: the case example of the North Pyrenean (Aquitaine, Bay of Biscay) Basins. Mar. Pet. Geol. 112, 104085. https://doi.org/10.1016/j.marpetgeo.2019.104085.
Ramboz, C., Charef, A., 1988. Temperature, pressure, burial history, and paleohydrology of the Les Malines, Pb-Zn deposit; reconstruction from aqueous inclusions in barite. Econ. Geol. 83, 784–800. https://doi.org/10.2113/gsecongeo.83.4.784.
Rhodes, D., Lantos, E.A., Lantos, J.A., Webb, R.J., Owens, D.C., 1984. Pine Point orebodies and their relationship to the stratigraphy, structure, dolomitization, and karstification of the Middle Devonian barrier complex. Econ. Geol. 79, 991–1055. https://doi.org/10.2113/gsecongeo.79.5.991.
Roig, J.-Y., Alabouvette, B., Collomb, P., Bogdanoff, S., Guerange-Lozes, J., Genna, A., Couture, J.-P., Monchoux, P., Ciszak, R., 2002. Notice explicative, Carte géol. France (1/50000), feuille Decazeville (859) 99.
Sabouraud, C.H., Macquar, J.-C., Rouvier, H., 1980. Les inclusions fluides, témoins et faux-témoins des conditions de dépôt. Quelques exemples pris dans les minéralisations de Pb, Zn, Ba, F du sud du Massif Central Français. Mineral. Deposita 15, 211–230. https://doi.org/10.1007/BF00206515.
Seal, R.R., 2006. Sulfur Isotope Geochemistry of Sulfide Minerals. Rev. Mineral. Geochem. 61, 633–677. https://doi.org/10.2138/rmg.2006.61.12.
Shelton, K.L., Rye, D.M., 1982. Sulfur isotopic compositions of ores from Mines Gaspe, Quebec: an example of sulfate-sulfide isotopic disequilibria in ore-forming fluids

with applications to other porphyry-type deposits. Econ. Geol. 77, 1688–1709. https://doi.org/10.2113/gsecongeo.77.7.1688.

Sizaret, S., Marcoux, E., Boyce, A., Jebrak, M., Stevenson, R., Ellam, R., 2009. Isotopic (S, Sr, Sm/Nd, D, Pb) evidences for multiple sources in the early Jurassic Chaillac F-Ba ore deposit (Indre, France). Bull. Soc. Geol. Fr. 180, 83–94. https://doi.org/10.2113/gssgfbull.180.2.83.

Sizaret, S., Marcoux, E., Jébrak, M., Touray, J.C., 2004. The Rossignol Fluorite Vein, Chaillac, France: Multiphase Hydrothermal activity and Intravein Sedimentation. Econ. Geol. 99, 1107–1122. https://doi.org/10.2113/gsecongeo.99.6.1107.

Stampfli, G.M., Borel, G.D., 2002. A plate tectonic model for the Paleozoic and Mesozoic constrained by dynamic plate boundaries and restored synthetic oceanic isochrons. Earth Planet. Sci. Lett. 196, 17–33. https://doi.org/10.1016/S0012-821X(01)00588-X.

Strzerzynski, P., Lenoir, L., Bessin, P., Bouat, L., 2020. Brittle tectonics and fluids overpressure during the early stage of the Bay of Biscay opening in the Jard-sur-Mer area, (northern Aquitaine Basin, France). Bull. Société Géologique Fr. 191, 38. https://doi.org/10.1051/bsgf/2020025.

Sverjensky, D.A., 1981. The origin of a Mississippi valley-type deposit in the Viburnum Trend, Southeast Missouri. Econ. Geol. 76, 1848–1872. https://doi.org/10.2113/gsecongeo.76.7.1848.

Sverjensky, D.A., 1986. Genesis of Mississippi Valley-type lead-zinc deposits. Annu. Rev. Earth Planet. Sci. 14, 177–199.

Turrillot, P., Augier, R., Monié, P., Faure, M., 2011. Late orogenic exhumation of the Variscan high-grade units (South Armorican Domain, western France), combined structural and 40Ar/39Ar constraints. Tectonics 30. https://doi.org/10.1029/2010TC002788.

Valenza, K., Moritz, R., Mouttaqi, A., Fontignie, D., Sharp, Z., 2000. Vein and karst barite deposits in the western Jebilet of Morocco: fluid inclusion and isotope (S, O, Sr) evidence for regional fluid mixing related to Central Atlantic rifting. Econ. Geol. 95, 587–606. https://doi.org/10.2113/gsecongeo.95.3.587.

Walter, B.F., Burisch, M., Fusswinkel, T., Marks, M.A., Steele-MacInnis, M., Wälle, M., Apukhtina, O.B., Markl, G., 2018. Multi-reservoir fluid mixing processes in rift-related hydrothermal veins, Schwarzwald. SW-Germany. J. Geochem. Explor. 186, 158–186. https://doi.org/10.1016/j.gexplo.2017.12.004.

Walter, B.F., Kortenbruck, P., Scharrer, M., Zeitvogel, C., Wälle, M., Mertz-Kraus, R., Markl, G., 2019. Chemical evolution of ore-forming brines – Basement leaching, metal provenance, and the redox link between barren and ore-bearing hydrothermal veins. A case study from the Schwarzwald mining district in SW-Germany. Chem. Geol. 506, 126–148. https://doi.org/10.1016/j.chemgeo.2018.12.038.

Wright, J.V., Haydon, R.C., McConachy, G.W., 1987. Sedimentary model for the giant Broken Hill Pb-Zn deposit, Australia. Geology 15, 598–602. https://doi.org/10.1130/0091-7613(1987)15%3C598:SMFTGB%3E2.0.CO;2.

Yardley, B.W.D., 2005. Metal Concentrations in Crustal Fluids and their Relationship to Ore Formation. Econ. Geol. 100, 613–632. https://doi.org/10.2113/gsecongeo.100.4.613.

Zheng, Y.-F., 1991. Sulphur isotopic fractionation between sulphate and sulphide in hydrothermal ore deposits: Disequilibrium vs equilibrium processes. Terra Nova 3, 510–516. https://doi.org/10.1111/j.1365-3121.1991.tb00186.x.